Journal of Asian Earth Sciences 113 (2015) 1082–1099

Contents lists available at ScienceDirect

Journal of Asian Earth Sciences

journal homepage: www.elsevier.com/locate/jseaes

Multiple magma evolution and ore-forming processes of the Hongge layered intrusion, SW China: Insights from Sr–Nd isotopes, trace elements and platinum-group elements

Mingyang Liao [a,b], Yan Tao [a,*], Xieyan Song [a], Yubang Li [a,b], Feng Xiong [a,b]

[a] State Key Laboratory of Ore Deposit Geochemistry, Institute of Geochemistry, Chinese Academy of Sciences, Guiyang 550002, China
[b] University of Chinese Academy of Sciences, Beijing 100049, China

ARTICLE INFO

Article history:
Received 15 October 2014
Received in revised form 16 March 2015
Accepted 17 March 2015
Available online 24 March 2015

Keywords:
Platinum group elements
Fe–Ti oxide deposit
Basalts
Hongge layered intrusion
Emeishan large igneous province

ABSTRACT

The Hongge layered intrusion (259 Ma), which is located in the inner zone of the Emeishan large igneous province (ELIP), is one of the most typical Fe–Ti–V ore deposits in the Pan–Xi area. Mafic–ultramafic layered intrusions of the ELIP have attracted a lot of attention lately because these intrusions host world class Fe–Ti–V oxide deposits plus interesting Cu–Ni–(PGE) mineralization which may have economic potential. This paper, reports new whole-rock major and trace element compositions, PGE abundances and Sr–Nd isotopic data for selected cumulate rocks and basalts. We use these data to investigate the nature of parental magmas and the controls on its evolution from the source mantle en route to the surface involving the Hongge ore-bearing intrusion. Two abrupt changes in Mt/Ilm and trace element ratios such as Ba/Th with depths in the Hongge layered intrusion indicate that this intrusion formed by at least two pluses of relatively primitive magma. The whole rock Sr–Nd isotopic data of basaltic and intrusive rocks plot in the region of Emeishan low-Ti basalts and the compositions of residual liquid (at ~1260 °C and 1155 °C) calculated by MELTS are similar to our actual high-Ti (BFQ-2) and low-Ti (BC-1) basltic samples, indicate they are co-magmatic rather than derivation from a distinct source. Total PGE abundances in the Hongge samples are extremely low, ranging from 0.5 to 10 ppb. Sulfide-bearing rocks in the Hongge intrusion and the nearby coeval Banfangqing and Baicao basalts have similar mantle-like Pd/Pt ratios (2–6) and extremely high Cu/Pd ratios (3×10^4 to 4×10^5), indicating that sulfide segregation took place at depth prior to emplacement at Hongge and eruption in this region. Sulfide saturation in the Hongge magma may have resulted from such crustal contamination event. Crystallization of silicate minerals under the anhydrous magma, magma hydration plus Fe–Ti enrichments in the parental magma are three critical factors for the formation of Fe–Ti oxide ore layers in the Hongge intrusion.

1. Introduction

Layered intrusions can provide valuable insights into understanding the genesis and evolution processes of mafic–ultramafic magma and the ore-forming processes associated with the formation of Cr, Fe–Ti–(V), and platinum group element (PGE) deposits, because they record the evolution history of magma associated with LIPs and passive continental margin (e.g. Wager and Brown, 1968; Irvine, 1975; Keays et al., 1999; Cabri, 2002). The ~260 Ma Emeishan large igneous province (ELIP) is one of the best exposed LIPs and hosts two types of temporally and spatially associated intrusions within it; these are: a. Fe–Ti–V oxide deposits in mafic–ultramafic layered intrusions, including the Panzhihua, Hongge, Taihe and Baima intrusions (Zhong et al., 2002, 2005; Zhou et al., 2005, 2008; Pang et al., 2008b); and b. Ni–Cu–(PGE) sulfide deposits in other mafic–ultramafic bodies, including the Limahe, Jinbaoshan, Baimazhai and Yangliuping intrusions (Song et al., 2003; Wang et al., 2006; Tao et al., 2007, 2008).

The Hongge intrusion in the Panzhihua–Xichang (Pan–Xi) area hosts the largest magmatic Fe–Ti–V oxide deposit in this region. It contains about 4572 Mt of oxide ores with 27 wt.% FeO, 10.6 wt.% TiO_2, and 0.24 wt.% V_2O_3 and presences of 0.5–3.5% disseminated sulfides (Yao et al., 1993; PXGT, 1987). Two main models including that fractional crystallization (Shellnutt et al., 2009, 2011, 2013; Shellnutt and Jahn, 2010) and liquid immiscibility (Zhou et al., 2005; Liu et al., 2014a, 2014b) were suggested as the main mechanisms for the Fe–Ti oxide ores in the Panxi district. Additionally, Ganino et al. (2008) proposed that the reaction between the mafic magma and the footwall limestone elevated

* Corresponding author. Tel./fax: +86 851 5891665.
E-mail address: taoyan@vip.gyig.ac.cn (Y. Tao).

http://dx.doi.org/10.1016/j.jseaes.2015.03.028
1367-9120/

the oxygen fugacity which results in early crystallization of Fe–Ti oxide and the formation of the Fe–Ti oxide ore layers in the Lower Zone of the Panzhihua intrusion. In addition, Bai et al. (2012a) has suggested that the Fe–Ti oxide ore layers in the Hongge intrusion were formed by injection of multiple pulse of Fe–Ti-rich magma and accumulation of titanomagnetite in a dynamic system. However, the precise mechanisms which concentrate million tons of Fe, Ti and V metals in this region are still debated and enigmatic.

PGE (Platinum-group elements) commonly are highly siderophile elements and their behavior can provide valuable information on the petrogenesis of mantle-derived igneous rocks and their source. The processes such as magma-rock interaction, sulfur saturation and sulfide segregation can be traced by PGE due to their high sensibility (Barnes et al., 1985; Keays, 1995; Lorand et al., 2008). The PGE content (total PGE: 0.09–63.5 ppb) in the Fe–Ti oxide layers of the Hongge intrusion appear to be very low (Bai et al., 2012b), which inspire us to use the low PGE concentrations to explore the nature of the mantle source and the sulfide saturation processes for the Hongge intrusion.

In this paper, we focus on the sulfide-enriched rocks, the Fe–Ti oxide ores and the associated basalts in the Hongge layered intrusion. New whole-rock major, trace element, PGE and Sr–Nd isotopic data of selected cumulate and basaltic rocks are reported to investigate the characteristic of parental magmas and to provide a better understanding of the evolution of the parental magma from the source mantle en route to the surface, more importantly, the critical factors required to constrain the formation of Fe–Ti ores within the Hongge layered intrusion.

2. Geological background

The Emeishan large igneous province (ELIP) is located between the western Yangtze Block and the eastern Tibetan Plateau and composed of massive flood basalts, numerous mafic–ultramafic layered intrusions, granites, syenites and other alkaline intrusions (Chung and Jahn, 1995; Fig. 1). The ELIP has attracted much attention because it contains numerous world-class V–Ti iron oxide deposits and is contemporaneous with the end-Guadalupian (~260 Ma) mass extinction (Shellnutt, 2014). The Emeishan continental flood basalts (ECFB), overlying the middle late Permian limestone of the Maokou formation, are exposed in the western Yangtze block with an area of approximately 5×10^5 km^2 (Xiao et al., 2004a,b). The basaltic sequence ranges in thickness from several hundred meters in the east to over 5 km in the west (Xu et al., 2001). The Emeishan basalts in the central ELIP include upper high-Ti (HT) basalts (TiO_2 > 2.5 wt.%, Ti/Y > 500) and lower low-Ti (LT) basalts (TiO_2 < 2.5 wt.%, Ti/Yb < 500), which are considered to have been derived from distinct mantle sources (He et al., 2010; Xiao et al., 2004a; Xu et al., 2001) or formed by fractional crystallization of different mineral phase from a common parental magma (c.f. Hao et al., 2004; Zhang, 2009; Dong and Zhang, 2009; Shellnutt and Jahn, 2011). Sporadic picrites associated with the high-Ti basalts were recorded from several localities (Chung and Jahn, 1995; Zhang et al., 2006). The recent study of Kamenetsky et al. (2012) indicated that the picrite lavas from thick stratigraphic successions at Binchuan and Yongsheng represent the low-Ti and high-Ti end-members of continental flood basalt magmatism, respectively. The high-Ti flood basalts have similar trace element and Sr–Nd isotope characteristic comparable with the OIB and are considered to be associated with a mantle plume (Song et al., 2001; Zhou et al., 2002, 2006).

In the central ELIP, numerous mafic–ultramafic layered intrusions containing Fe–Ti oxide deposits and Cu–Ni–(PGE) sulfide mineralization are exposed in the Pan–Xi area that has been controlled by a series of N–S-trending faults. These intrusions are distributed along the 200-km-long rift belt, including the Hongge (259 ± 1.3 Ma, Zhong and Zhu, 2006), and Xinjie (259 ± 3 Ma, Zhou et al., 2002) mafic–ultramafic intrusions and the Panzhihua (261 ± Ma, Shellnutt et al., 2011), Baima (261 ± 2 Ma, Shellnutt et al., 2009) and Taihe (262 ± 3 Ma, Guo et al., 2004) mafic intrusions. The relatively small sill-like intrusive bodies located in the central ELIP (e.g., Limahe, Tao et al., 2009) and outer zone of ELIP (Baimazhai, Wang et al., 2006; Yangliuping, Song et al., 2003) host Cu–Ni–(PGE) sulfide mineralization.

3. Geology and petrography of the Hongge layered intrusion

The 15 km-long, 3–5 km-wide, 1.2 km-thick and NNE-striking elongated lopolith Hongge Fe–Ti–V oxide ore deposit which crops out over an area of about 60 km^2 is located to the northeast of Panzhihua city (Fig. 1). The Hongge intrusion intersects the dolomitic limestones of the Sinian Dengying Formation and granitic gneisses of the Neoproterozoic Kangding Complex. The Dengying Formation is composed of dolomitic limestone, which is metamorphosed to marble in place adjacent to the layered intrusion. The west and north contact zones of the intrusion were intruded by the late Permian alkaline granites and alkaline syenites (Fig. 1; Zhang et al., 1999). The Hongge intrusion was surrounded and cut by ~255.2 ± 3.6 Ma later Permian granite and syenite (Xu et al., 2008). Part of the intrusion at the northeast corner is overlain by ~180 m-thick basaltic sequence of the ECFB (Fig. 1c). Based on the cumulus minerals and lithologic textures (Figs. 2 and 3; Zhong et al., 2002), the strongly differentiated Hongge intrusion was divided into three lithologic zones from the base to the top: the lower olivine clinopyroxenite zone (LOZ), the middle clinopyroxenite zone (MCZ) and the upper gabbro zone (UGZ). The LOZ and MCZ are characterized by the appearance and disappearance of olivine whereas the UGZ is defined by the appearance of abundant euhedral apatite. The massive Fe–Ti oxide bodies mainly occur in the upper part of the LOZ and the lower part of the MCZ (Zhong et al., 2002) as layers with different thickness contacts with the intrusion.

The thickness of LOZ is about 340 m. It is composed of medium- to fine-grained rocks containing cumulus olivine, magnetite and ilmenite and minor chromite, and intercumulus clinopyroxene and hornblende within its lower part. The Fe–Ti oxide minerals occur as inclusions in the cumulus phases clearly indicate they precipitated early than silicate minerals (primocrysts) including olivine and clinopyroxene. Fine-grained magnetite and ilmenite mainly occur in the interstitial spaces between olivine and clinopyroxene. The MCZ comprises lherzolite and olivine clinopyroxene at the bottom and clinopyroxenite at the top, which contains cumulus plagioclase. The MCZ has more interstitial magnetite and ilmenite than the LOZ. Minor amounts of Cr-spinel and olivine locate in the rocks beneath the massive Fe–Ti oxide layers. The abundance of plagioclase increases progressively from the base to the top in the MCZ and UGZ. Some clinopyroxene crystals in the base of the MCZ contain exsolved Fe–Ti oxides. The MCZ contains the largest and richest economic Fe–Ti–V oxide layers. Also, platinum-group element-rich horizons were documented in the lower parts of the LOZ and the MCZ, which are below a thick magnetite horizon. The average total PGE concentration in the PGE-enriched horizon within the LOZ and the MCZ is 0.354 ppm and 0.533 ppm, respectively (Liang et al., 1998). Pyrrhotite is the major sulfide mineral, accounting for ~90% of the sulfide assemblages. Sperrylite, vincentite and laurite are the most common platinum-group minerals (PGM) within the intrusion (Liang et al., 1998). The 527- to 1346-m-thick UGZ is composed of plagioclase, clinopyroxene, with minor olivine in its base.

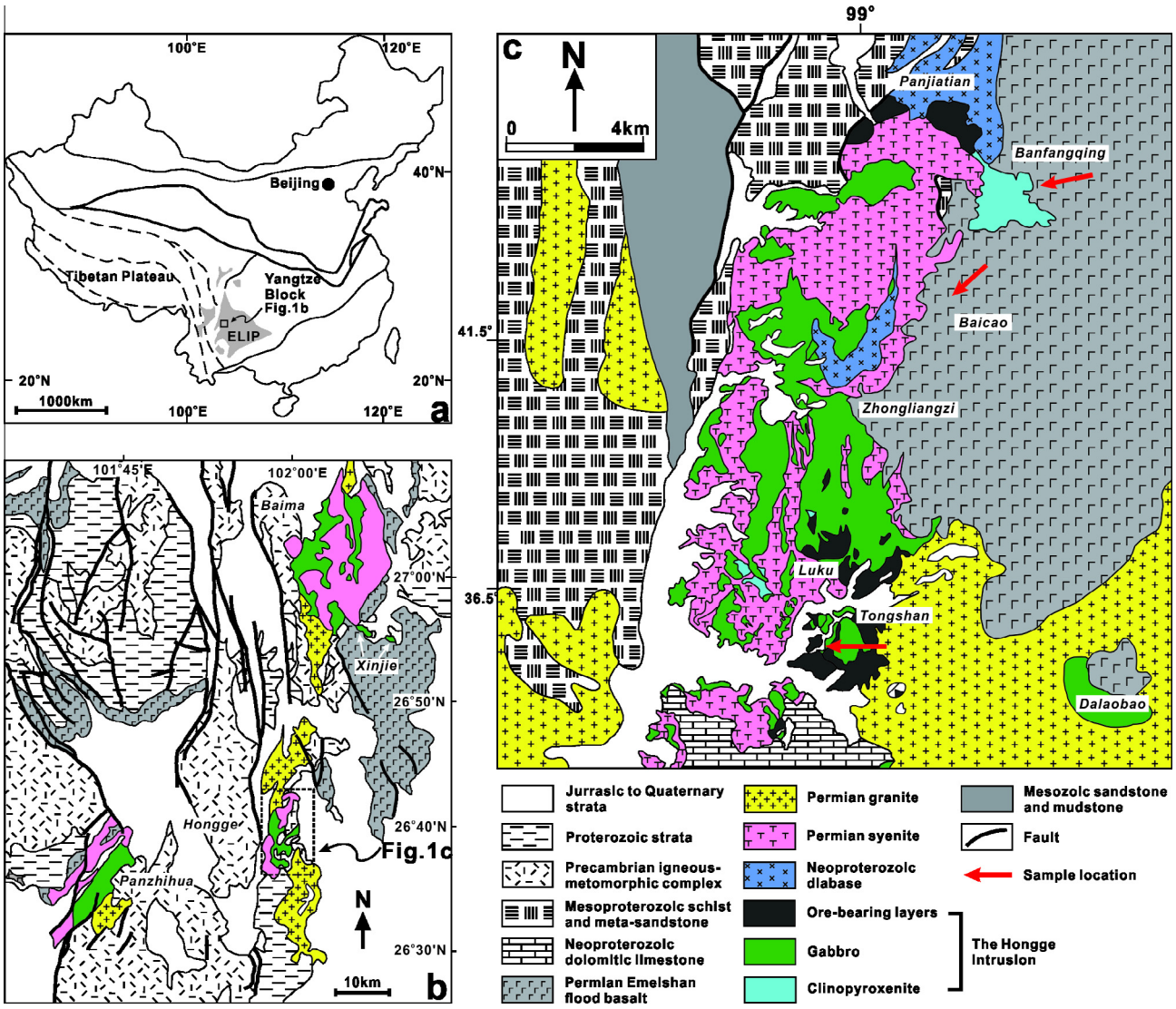

Fig. 1. Geological map showing the distribution of the Emeishan large igneous province (a; ELIP), the distribution of the major Fe–Ti–V oxide-bearing intrusions in the Panxi region (b; modified after Pang et al., 2008a), and goelogical map of the Hongge intrusion (c; modified after Sichuan Geological Survey 2010).

The general crystallization order inferred from cumulus phases in the LOZ and MCZ is: olivine → olivine + chromite + Fe–Ti oxides → olivi ne + clinopyroxene + Fe–Ti oxides → clinopyrox ene + Fe–Ti oxides. In addition, the order inferred from cumulus stratigraphy of the UGZ is: clinopyroxene + plagioclase + Fe–Ti oxides + apat ite → clinopyroxene + plagioclase + apatite. The apatite gabbro generally contains <15% Fe–Ti oxides, 20–45% clinopyroxene, 40–50% plagioclase, 5–7% apatite and <3–5% hornblende (locally up to 10%). Minor granophyre and felsic pegmatite occur as dikes or lenses within this zone and cumulus plagioclase content increases upwards as the rock change from melagabbro to leucogabbro.

4. Sampling and analytical methods

The samples analyzed in this study are collected from the surface located in the southern and northwestern part of the Hongge intrusion (Fig. 1c). Thirty-one samples (HG0–6, 8–28, 30–32) including olivine clinopyroxenite, clinopyroxenite, gabbro and massive ores from the lower zone to upper zone were collected from the surface of Tongshan and fifteen basalts (BC1–4, BFQ1–11) were collected from the Baicao and the Banfangqing areas respectively. The stratigraphic positions of these samples are shown in Fig. 3.

Major element compositions of the samples were analyzed by X-ray fluorescence (XRF) spectrometry at State Key Laboratory of Ore Deposit Geochemistry (SKLODG, Institute of Geochemistry, Chinese Academy of Sciences in Guiyang). The analytical precision is better than 5% relative standard deviation. Trace elements of whole rocks were determined using a Perkin–Elmer EIAN DCR II ICP-MS at SKLODG. The powdered sample (50 mg) were dissolved with HF + HNO_3 mixture in high-pressure Teflon bombs for 48 h at ~190 °C (Qi et al., 2000). 500 mg/ml Rh was used as internal standard to monitor signal drift during analysis. We use the international standards GBPG-1, OU-6, and the Chinese National standards GSR-1 and GSR-3 to monitor the analytical accuracy. The accuracy and precision for the ICP-MS analyses is generally better than 10% relative standard deviation. The compositions of major and trace elements are listed in Table 1.

Rb–Sr and Sm–Nd isotopic analyses of whole-rock samples were spiked and dissolved with HF + HNO_3 acid in Teflon bombs. We apply the conventional cation-exchange techniques to separate the Sm and Nd. The isotopic measurements were performed on a Thermal Ionization Mass Spectrometry (TIMS)-Triton at the

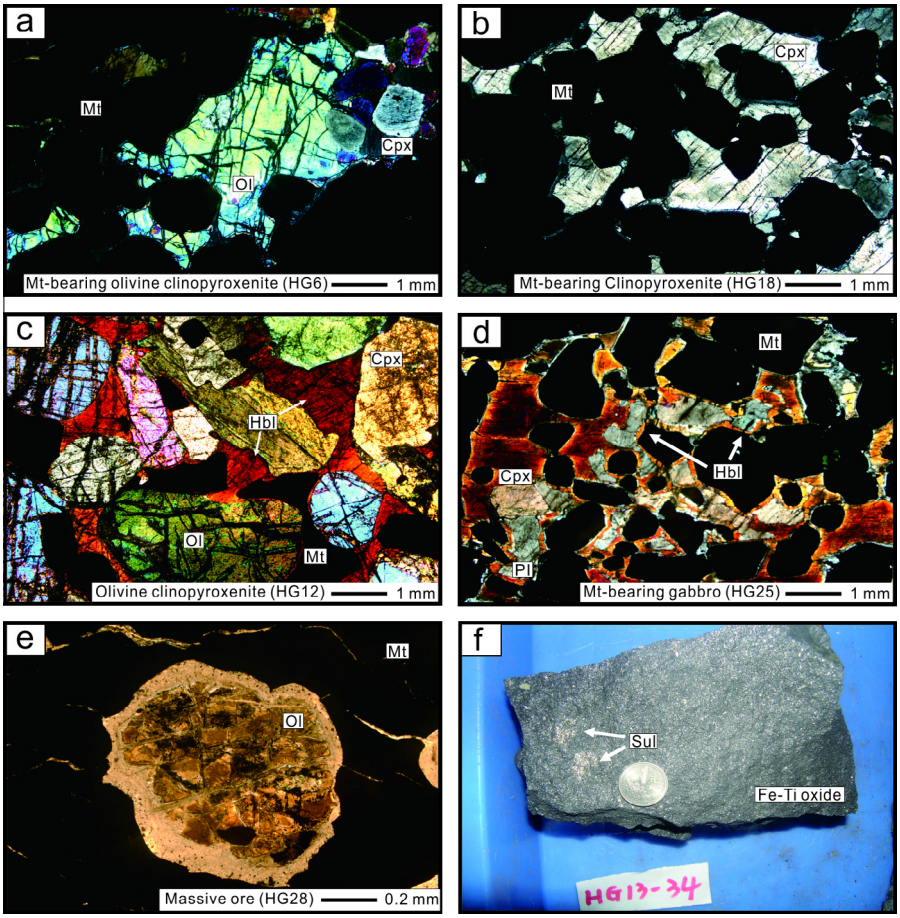

Fig. 2. Photomicrographs and field photographs of samples showing representative rock textures in the Hongge layered intrusion. (a) Olivine clinopyroxenite. (b) Mt-bearing Clinopyroxenite. (c) Olivine clinopyroxenite contain Hornblende. (d) Mt-bearing gabbro. (e) Olivine in massive ore. (f) Disperse sulfide in Fe–Ti oxide. Ol = Olivine, Cpx = Clinopyroxene, Pl = Plagioclase, Sul = Sulfide. Mt = Magnetite, Hbl = Hornblende. The photomicrographs of a–e are taken under cross-polarized light.

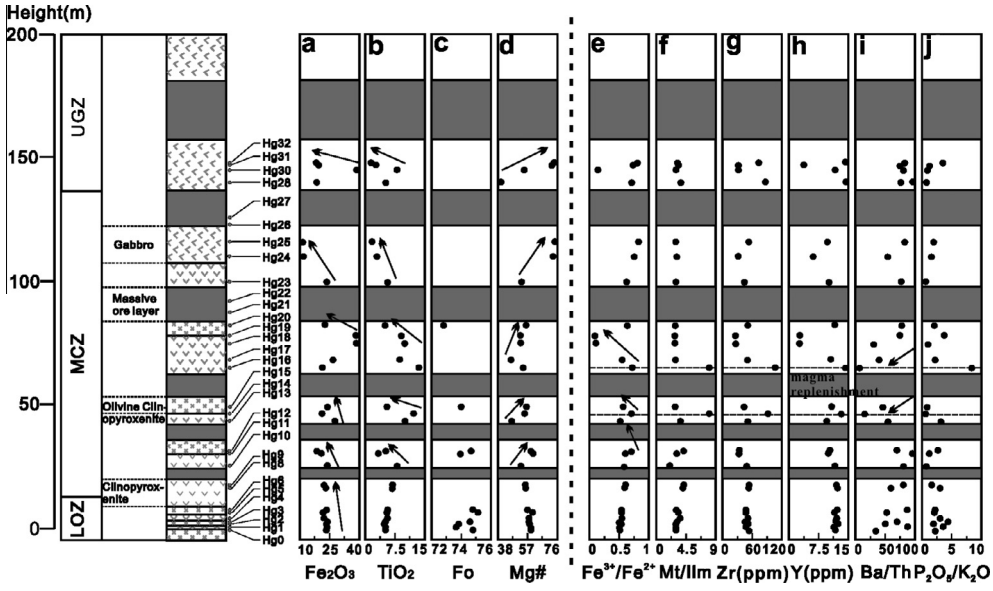

Fig. 3. Stratigraphic column of the Hongge layered intrusion, showing the subdivision and chemical variation of major element oxides and trace elements from the top LOZ to UGZ.

Table 1
Major and trace element compositions of the rocks from the Hongge intrusion and the Banfangqing and Baicao basalts.

	Lower zone							Middle zone				
Sample	HG0	HG1	HG2	HG3	HG4	HG5	HG6	HG8	HG9	HG10	HG11	HG12
Rock type	Ocp	Cpx	Ocp	Ocp	Cpx	Ocp	Ocp	Cpx	Cpx	Cpx	Ocp	Ocp
Height (m)	0.00	0.50	3.00	3.50	4.00	6.50	7.00	12.00	13.00	25.00	30.00	31.00
Major oxides (wt.%)												
SiO_2	36.10	35.22	36.86	34.94	35.25	36.42	35.57	36.24	36.73	35.18	40.79	42.13
TiO_2	4.99	4.86	4.87	5.25	6.19	5.55	5.64	7.06	7.07	7.61	3.58	4.50
Al_2O_3	3.60	3.51	3.76	3.64	3.72	3.51	4.21	3.74	3.76	3.52	3.36	3.85
Fe_2O_3	23.78	23.20	23.14	24.12	22.69	22.63	24.20	23.06	22.19	24.32	21.47	18.81
MnO	0.21	0.20	0.20	0.21	0.20	0.20	0.20	0.18	0.17	0.17	0.19	0.16
MgO	19.26	18.79	17.88	17.95	16.96	18.48	16.31	14.49	13.96	13.64	17.74	14.48
CaO	11.38	11.10	13.32	12.39	12.99	12.37	13.20	14.17	14.88	14.41	11.44	15.53
Na_2O	0.25	0.24	0.21	0.32	0.22	0.23	0.48	0.30	0.30	0.25	0.32	0.32
K_2O	0.05	0.05	0.02	0.04	0.03	0.03	0.17	0.04	0.04	0.02	0.07	0.04
P_2O_5	0.12	0.12	0.09	0.08	0.11	0.10	0.09	0.09	0.09	0.05	0.09	0.02
LOI	0.61	3.36	1.08	0.41	1.06	1.14	0.82	0.51	0.39	0.36	1.73	0.93
Mg-No.	62	62	61	60	60	62	57	56	56	53	62	61
Total	99.74	97.30	100.36	98.93	98.34	99.53	100.08	99.37	99.20	99.17	99.04	99.84
P_2O_5/K_2O	2.31	2.31	3.95	2.11	4.36	3.05	0.53	2.01	2.28	2.83	1.32	0.61
Trace element (ppm)												
Cu	34.90	34.10	30.10	30.50	37.00	35.50	33.10	48.90	77.30	64.30	195.00	142.00
Cr	1620	1790	1910	1660	1710	1790	1700	1390	1340	1150	1120	1140
La	7.31	5.64	5.23	4.65	5.40	4.86	4.94	5.08	5.06	3.63	4.57	3.31
Ce	18.50	15.30	15.50	13.70	15.30	14.10	14.10	14.70	15.30	11.60	12.60	10.80
Pr	3.20	2.75	2.95	2.60	2.84	2.65	2.65	2.76	2.89	2.32	2.22	2.18
Nd	16.40	14.50	15.60	14.20	15.30	14.30	14.50	15.00	15.80	12.80	11.80	12.30
Sm	4.31	3.81	4.37	3.97	4.12	4.02	4.16	4.17	4.46	3.72	3.14	3.59
Eu	1.38	1.30	1.49	1.32	1.39	1.29	1.35	1.42	1.44	1.26	1.08	1.23
Gd	4.51	4.01	4.43	3.99	4.13	3.89	4.16	4.28	4.29	3.70	3.33	3.70
Tb	0.60	0.53	0.63	0.57	0.59	0.56	0.59	0.62	0.64	0.52	0.44	0.51
Dy	2.89	2.66	3.09	2.71	2.76	2.65	2.86	2.92	2.97	2.56	2.26	2.51
Ho	0.56	0.49	0.57	0.51	0.52	0.52	0.53	0.54	0.55	0.49	0.41	0.46
Er	1.31	1.14	1.28	1.20	1.17	1.14	1.24	1.21	1.27	1.09	0.94	1.05
Tm	0.14	0.13	0.15	0.14	0.14	0.14	0.14	0.14	0.16	0.13	0.11	0.12
Yb	0.90	0.79	0.88	0.79	0.84	0.79	0.86	0.83	0.92	0.73	0.64	0.69
Lu	0.12	0.10	0.12	0.10	0.11	0.10	0.12	0.11	0.12	0.09	0.09	0.09
ΣREE	62.12	53.14	56.28	50.44	54.60	51.00	52.20	53.77	55.86	44.63	43.62	42.55
V	461	533	559	566	565	525	605	657	659	711	482	576
Ni	533.00	693.00	621.00	609.00	515.00	603.00	571.00	314.00	334.00	358.00	412.00	346.00
Cu	34.90	34.10	30.10	30.50	37.00	35.50	33.10	48.90	77.30	64.30	195.00	142.00
Ge	1.62	1.59	1.83	1.72	1.74	1.81	1.74	1.73	1.76	1.67	1.58	1.74
Rb	2.04	2.06	1.05	1.06	0.91	1.10	1.01	1.99	1.12	0.86	1.66	0.64
Sr	160	143	123	120	114	127	117	132	140	114	113	116
Y	12.70	11.10	13.00	11.70	12.10	11.60	12.10	12.40	12.80	11.10	9.12	10.20
Zr	56.70	47.30	49.70	47.30	53.20	48.10	49.50	56.70	58.00	50.80	33.80	37.00
Nb	7.01	5.89	4.32	4.45	7.72	5.96	4.92	7.52	7.89	7.42	3.10	2.50
Ba	24	31	14	18	15	20	17	24	21	15	22	7
Hf	2.18	1.95	2.10	1.95	2.17	1.97	2.10	2.24	2.31	2.05	1.43	1.80
Ta	0.61	0.52	0.38	0.41	0.66	0.53	0.43	0.68	0.71	0.69	0.28	0.26
Th	0.69	0.36	0.28	0.25	0.29	0.23	0.27	0.28	0.25	0.14	0.31	0.12
U	0.17	0.12	0.08	0.07	0.08	0.08	0.08	0.09	0.07	0.05	0.12	0.05
Ba/Th	34	85	51	73	54	89	63	84	84	107	70	58
La/Nb	1.04	0.96	1.21	1.04	0.70	0.82	1.00	0.68	0..64	0.49	1.47	1.32
Th/Ta	1.14	0.69	0.72	0.62	0.43	0.43	0.62	0.42	0.35	0.20	1.12	0.45

	Middle zone										Upper zone	
Sample	HG13	HG14	HG15	HG16	HG17	HG18	HG19	HG20	HG21	HG22	HG23	HG24
Rock type	Cpx	Cpx	Ocp	Cpx	Cpx	Mt-Cpx	Mt-Cpx	Ocp	Ore	Ore	Ocp	Cpx
Height (m)	44.00	47.00	49.00	65.00	68.00	75.00	78.00	82.00	87.00	90.00	102.00	110.00
Major oxides (wt.%)												
SiO_2	33.77	36.32	37.26	34.83	34.79	22.15	23.28	38.16	16.85	11.26	36.31	41.71
TiO_2	9.17	12.65	5.27	12.89	8.55	9.43	8.93	4.88	21.49	13.45	5.52	3.12
Al_2O_3	3.90	3.81	3.97	3.99	4.39	3.10	3.23	4.17	3.15	3.48	4.60	4.16
Fe_2O_3	28.01	19.55	24.05	20.24	27.82	38.23	38.11	21.56	44.67	56.07	22.87	13.74
MnO	0.20	0.19	0.19	0.18	0.19	0.24	0.25	0.17	0.29	0.21	0.16	0.14
MgO	12.64	12.26	15.47	12.06	11.88	20.77	21.35	13.84	7.24	13.75	11.84	18.87
CaO	12.42	14.17	12.23	14.02	13.38	1.73	1.86	14.47	6.08	0.08	12.88	17.87
Na_2O	0.29	0.21	0.27	0.22	0.28	0.46	0.08	0.31	0.17	0.02	0.32	0.08
K_2O	0.05	0.04	0.05	0.03	0.04	0.08	0.03	0.06	0.02	0.01	0.06	0.01
P_2O_5	0.05	0.10	0.17	0.26	0.08	0.08	0.13	0.12	0.03	0.03	0.07	0.42
LOI	Trace	0.71	1.07	0.64	0.01	2.59	2.75	0.77	Trace	1.95	5.72	0.08
Mg-No.	47	56	56	54	46	52	53	56	24	33	51	73
Total	100.50	99.29	98.93	98.72	101.40	96.27	97.26	97.74	100.00	98.36	94.61	100.13
P_2O_5/K_2O	1.10	2.67	3.16	8.57	2.02	1.08	3.75	2.04	1.14	32.42	0.61	1.42

Table 1 (*continued*)

	Middle zone										Upper zone	
Sample	HG13	HG14	HG15	HG16	HG17	HG18	HG19	HG20	HG21	HG22	HG23	HG24
Rock type	Cpx	Cpx	Ocp	Cpx	Cpx	Mt-Cpx	Mt-Cpx	Ocp	Ore	Ore	Ocp	Cpx
Height (m)	44.00	47.00	49.00	65.00	68.00	75.00	78.00	82.00	87.00	90.00	102.00	110.00
Trace element (ppm)												
Cu	314.00	246.00	101.00	258.00	225.00	65.10	68.00	152.00	141.00	189.00	199.00	117.00
Cr	1620	163	1150	135	475	3850	3750	1220	82	6300	885	2360
La	3.41	6.54	6.09	9.82	5.12	2.22	2.83	6.15	1.01	0.54	4.91	2.49
Ce	10.80	18.20	15.60	23.80	14.40	4.81	6.07	16.40	3.26	1.15	13.40	7.08
Pr	2.10	3.24	2.69	3.98	2.60	0.69	0.89	2.89	0.66	0.17	2.43	1.32
Nd	11.80	17.40	14.00	20.30	13.90	3.27	4.13	15.40	3.65	0.90	12.90	7.36
Sm	3.45	4.83	3.73	5.28	3.77	0.74	0.91	4.03	1.20	0.21	3.55	2.06
Eu	1.09	1.55	1.22	1.72	1.27	0.24	0.30	1.36	0.39	0.06	1.17	0.70
Gd	3.34	4.89	3.61	5.33	3.88	0.70	0.87	4.03	1.17	0.19	3.34	2.08
Tb	0.47	0.68	0.52	0.76	0.54	0.10	0.13	0.57	0.17	0.03	0.51	0.29
Dy	2.31	3.36	2.43	3.49	2.60	0.46	0.58	2.74	0.82	0.16	2.37	1.44
Ho	0.44	0.64	0.45	0.68	0.47	0.09	0.11	0.51	0.16	0.03	0.44	0.28
Er	1.02	1.41	1.05	1.56	1.11	0.23	0.28	1.16	0.35	0.09	1.00	0.61
Tm	0.11	0.17	0.12	0.18	0.12	0.03	0.03	0.14	0.04	0.01	0.11	0.07
Yb	0.69	1.02	0.68	1.07	0.79	0.18	0.21	0.80	0.28	0.06	0.68	0.44
Lu	0.10	0.15	0.09	0.15	0.10	0.03	0.03	0.10	0.04	0.01	0.09	0.06
ΣREE	41.13	64.07	52.28	78.12	50.68	13.78	17.35	56.27	13.19	3.60	46.91	26.28
V	909	525	674	548	903	1150	1160	649	1530	1700	803	1160
Ni	318.00	349.00	395.00	518.00	215.00	752.00	599.00	252.00	83.20	1030.00	204.00	443.00
Cu	314.00	246.00	101.00	258.00	225.00	65.10	68.00	152.00	141.00	189.00	199.00	117.00
Ge	1.72	1.46	1.56	1.49	1.54	0.92	0.98	1.67	1.01	1.09	1.67	1.37
Rb	0.80	0.54	1.64	0.57	0.77	0.81	0.98	1.82	0.46	0.33	1.43	0.66
Sr	105	96	111	93	112	40	48	160	36	8	132	72
Y	9.60	13.70	10.40	15.10	10.70	2.11	2.69	11.50	3.72	0.66	9.77	6.07
Zr	50.80	92.30	43.80	105.00	53.10	27.40	25.10	48.90	60.10	15.40	44.90	31.80
Nb	9.71	25.20	4.80	26.70	7.69	7.02	6.10	5.26	14.10	3.18	3.90	4.97
Ba	13	7	16	7	11	17	19	38	6	15	23	11
Hf	2.07	3.49	1.85	3.63	2.19	0.89	0.88	1.93	2.34	0.61	1.93	1.36
Ta	0.94	2.37	0.44	2.47	0.75	0.64	0.53	0.44	1.77	0.38	0.34	0.47
Th	0.18	0.42	0.34	0.98	0.39	0.22	0.25	0.45	0.07	0.07	0.41	0.14
U	0.05	0.13	0.10	0.26	0.12	0.07	0.09	0.13	0.04	0.07	0.12	0.05
Ba/Th	70	17	46	7	28	75	77	83	83	206	57	82
La/Nb	0.35	0.26	1.27	0.37	0.67	0.32	0.46	1.17	1.26	0.50	0.25	1.88
Th/Ta	0.19	0.18	0.79	0.40	0.52	0.35	0.46	1.03	0.04	0.19	1.19	0.29
	Upper zone						Baicao				Banfangiqng	
Sample	HG25	HG26	HG27	HG28	HG30	HG31	HG32	BC-1	BC-2	BC-3	BC-4	BFQ-1
Rock type	Gb	Ore	Mt-Gb	Gb	Mt-Gb	Gb	Gb	LT	LT	HT	HT	HT
Height (m)	115.00	119.00	125.00	139.00	145.00	147.00	148.00					
Major oxides (wt.%)												
SiO_2	45.88	6.35	5.90	28.03	24.03	39.23	44.55	48.14	48.75	53.16	51.53	45.89
TiO_2	2.35	16.81	16.89	5.11	8.01	2.96	2.25	1.76	1.77	3.69	3.68	3.73
Al_2O_3	3.16	3.94	4.11	11.59	3.12	3.93	3.53	15.61	15.69	16.28	15.86	12.41
Fe_2O_3	11.49	64.60	65.86	18.15	39.39	13.17	11.80	10.69	10.83	7.63	9.56	15.54
MnO	0.12	0.31	0.31	0.21	0.25	0.13	0.11	0.17	0.16	0.24	0.25	0.22
MgO	18.68	7.86	7.07	15.69	23.84	17.95	18.04	6.04	6.14	3.45	3.92	5.47
CaO	18.53	0.16	0.04	13.78	0.61	16.91	18.38	10.09	9.21	8.80	9.11	11.96
Na_2O	0.09	0.06	0.09	1.24	0.08	0.05	0.03	3.33	3.76	4.74	4.45	2.83
K_2O	0.04	0.02	0.02	1.26	0.03	0.01	0.01	1.23	1.31	1.56	1.40	0.82
P_2O_5	0.02	0.02	0.01	1.80	0.07	0.41	0.03	0.40	0.40	0.53	0.55	0.70
LOI	0.15	0.13	0.08	2.32	0.54	5.71	0.21	3.10	2.89	0.58	0.25	1.15
Mg-No.	76	20	18	63	56	73	75	53	53	47	45	41
Total	100.36	100.13	100.30	96.86	99.44	94.76	98.74	100.55	100.92	100.66	100.57	100.72
P_2O_5/K_2O	1.99	31.27	3.12	0.69	0.77	1.24	3.58					
Trace element (ppm)												
Cu	212.00	162.00	221.00	60.50	19.80	499.00	492.00	67.63	64.12	40.44	54.56	52.19
Cr	177	1440	4630	63	51	4640	946	76	63	46	39	65
La	2.55	2.93	0.27	30.80	3.10	1.92	11.80	29.50	29.30	64.80	237.00	19.00
Ce	8.20	8.28	0.60	68.40	7.83	3.46	28.50	58.60	57.90	140.00	431.00	43.10
Pr	1.74	1.56	0.08	10.60	1.57	0.50	4.60	6.72	6.66	17.50	44.10	5.97
Nd	10.20	8.41	0.35	49.90	9.07	2.21	22.50	26.90	26.90	72.60	153.00	27.90
Sm	3.07	2.36	0.08	11.00	2.78	0.56	5.47	4.93	5.07	13.90	22.60	5.92
Eu	1.00	0.83	0.03	3.73	1.43	0.18	1.69	1.74	1.69	4.05	4.64	2.68
Gd	3.19	2.41	0.08	9.87	2.84	0.50	5.05	4.71	4.78	11.56	18.84	5.53
Tb	0.44	0.35	0.01	1.35	0.43	0.07	0.72	0.74	0.76	1.84	2.62	0.81
Dy	2.17	1.71	0.06	6.04	2.22	0.37	3.38	4.21	4.22	9.55	12.40	4.11
Ho	0.38	0.31	0.01	1.14	0.43	0.07	0.64	0.81	0.88	1.74	2.25	0.76
Er	0.87	0.68	0.03	2.69	1.07	0.16	1.49	2.40	2.44	4.61	6.23	1.91
Tm	0.10	0.08	0.00	0.29	0.14	0.02	0.17	0.35	0.34	0.61	0.81	0.22

(*continued on next page*)

Table 1 (*continued*)

	Upper zone						Baicao				Banfangiqng	
Sample	HG25	HG26	HG27	HG28	HG30	HG31	HG32	BC-1	BC-2	BC-3	BC-4	BFQ-1
Rock type	Gb	Ore	Mt-Gb	Gb	Mt-Gb	Gb	Gb	LT	LT	HT	HT	HT
Height (m)	115.00	119.00	125.00	139.00	145.00	147.00	148.00					
Yb	0.62	0.45	0.03	1.71	0.81	0.12	0.89	2.10	2.13	3.48	4.97	1.34
Lu	0.08	0.06	0.01	0.23	0.11	0.02	0.12	0.31	0.31	0.49	0.75	0.19
ΣREE	34.62	30.42	1.64	197.77	33.81	10.15	87.01	144.02	143.39	346.73	941.21	119.45
V	868	313	2190	431	368	1020	295	246	241	238	251	403
Ni	119.00	424.00	742.00	71.30	113.00	1170.00	1070.00	55.80	52.20	18.60	13.20	75.90
Cu	212.00	162.00	221.00	60.50	19.80	499.00	492.00	67.63	64.12	40.44	54.56	52.19
Ge	1.43	1.48	0.96	1.37	1.51	0.93	1.57	1.58	1.58	2.25	2.58	1.79
Rb	0.50	0.42	0.12	34.30	39.50	0.63	0.60	76.60	86.30	45.20	44.00	5.64
Sr	88	55	4	992	1260	14	68	887	905	834	810	520
Y	9.03	8.20	0.79	27.40	11.20	3.82	16.10	22.70	22.90	47.00	61.20	19.10
Zr	55.10	31.70	20.40	86.90	31.60	30.80	72.80	129.00	129.00	320.00	865.00	61.70
Nb	10.30	0.72	3.53	16.40	5.32	2.75	5.91	20.30	20.30	133.00	194.00	17.10
Ba	15	4	2	604	425	12	5	545	563	702	679	334
Hf	2.39	1.29	0.74	2.64	1.25	0.98	2.47	3.22	3.23	7.96	19.20	2.03
Ta	1.04	0.07	0.41	1.20	0.47	0.24	0.43	1.09	1.06	5.11	6.95	1.07
Th	0.08	0.19	0.04	1.56	0.03	0.13	0.91	3.76	3.84	3.92	29.40	0.88
U	0.05	0.09	0.04	0.40	0.04	0.16	0.22	0.78	0.78	1.43	4.66	0.25
Ba/Th	185	23	56	387	16,537	89	6	145	147	179	23	378
La/Nb	0.58	0.70	2.00	4.09	0.08	0.07	1.17					
Th/Ta	0.08	2.77	0.10	1.30	0.05	0.54	2.11					

	Banfangqing									
Sample	BFQ-2	BFQ-3	BFQ-4	BFQ-5	BFQ-6	BFQ-7	BFQ-8	BFQ-9	BFQ-10	BFQ-11
Rock type	HT	HT	HT	HT	HT	LT	HT	LT	HT	HT
Height (m)										
Major oxides (wt.%)										
SiO_2	45.57	48.34	45.03	45.18	45.23	49.11	45.02	48.87	45.55	50.27
TiO_2	3.96	3.36	3.65	3.77	3.73	1.20	4.25	2.05	4.02	3.88
Al_2O_3	12.53	14.09	11.57	11.70	12.05	16.03	12.10	14.63	15.11	14.34
Fe_2O_3	15.87	13.81	15.09	15.44	15.04	10.87	16.08	13.11	15.40	13.09
MnO	0.22	0.20	0.21	0.22	0.21	0.17	0.25	0.20	0.21	0.21
MgO	5.22	5.58	8.61	8.79	8.06	6.85	8.04	6.69	6.56	4.05
CaO	10.26	8.81	11.24	11.59	10.21	8.60	11.69	9.12	11.20	10.12
Na_2O	3.26	4.24	3.95	3.65	4.03	3.50	1.18	1.15	1.16	2.70
K_2O	0.96	1.32	0.61	0.41	1.17	1.26	0.85	1.27	0.67	0.94
P_2O_5	0.78	0.42	0.36	0.36	0.34	0.38	0.42	0.46	0.34	0.47
LOI	1.25	0.79	0.04	0.15	1.28	2.96	0.62	2.07	0.25	0.76
Mg-No.	40	45	53	53	52	56	50	51	46	38
Total	99.89	100.96	100.37	101.27	101.34	100.93	100.49	99.62	100.48	100.82
Trace element (ppm)										
Cu	41.32	41.93	31.84	40.35	32.54	66.84	31.32	68.60	19.04	44.12
Cr	31	87	266	268	288	66	259	87	43	45
La	21.50	55.30	20.60	19.30	18.00	27.40	24.60	22.40	15.40	47.70
Ce	48.00	115.00	51.40	48.70	46.10	54.60	60.30	43.10	36.40	102.00
Pr	6.56	14.00	7.19	7.03	6.62	6.29	8.29	5.01	4.97	13.00
Nd	30.60	56.40	34.10	33.60	32.30	25.10	39.20	21.20	24.10	53.90
Sm	6.61	10.30	7.61	7.78	7.39	4.62	8.58	4.42	5.86	10.30
Eu	3.03	3.18	2.55	2.60	2.45	1.71	2.74	1.59	2.13	3.17
Gd	5.90	8.52	7.15	7.06	6.74	4.45	7.92	4.66	5.65	8.72
Tb	0.91	1.28	1.08	1.12	1.11	0.77	1.25	0.79	0.88	1.29
Dy	4.59	5.95	5.79	5.88	5.64	4.16	6.27	4.74	4.58	6.30
Ho	0.82	1.11	1.06	1.08	1.04	0.85	1.18	0.97	0.87	1.20
Er	2.09	2.99	2.87	2.82	2.69	2.44	3.12	2.75	2.22	3.19
Tm	0.26	0.37	0.35	0.35	0.34	0.33	0.41	0.40	0.29	0.42
Yb	1.42	2.33	2.06	2.09	2.08	2.04	2.43	2.39	1.76	2.45
Lu	0.22	0.31	0.30	0.30	0.30	0.31	0.35	0.37	0.24	0.36
ΣREE	132.52	277.05	144.1	139.72	132.8	135.07	166.63	114.79	105.36	254
V	404	341	389	404	412	233	388	318	423	348
Ni	64.00	17.00	68.10	67.60	70.50	61.00	62.40	61.90	24.20	27.00
Cu	41.32	41.93	31.84	40.35	32.54	66.84	31.32	68.60	19.04	44.12
Ge	1.66	1.92	1.95	2.01	1.93	1.45	2.12	1.52	1.84	2.06
Rb	7.61	41.40	27.20	16.00	74.00	61.20	41.00	43.50	33.40	40.90
Sr	860	1070	606	588	673	776	648	448	603	1080
Y	21.00	27.80	26.20	26.20	25.50	22.70	29.20	27.50	22.60	30.00
Zr	67.00	207.00	94.40	87.40	97.30	119.00	93.10	99.60	90.30	179.00
Nb	18.60	62.30	30.90	31.30	30.00	18.20	34.30	20.90	27.50	66.80
Ba	747	547	200	157	215	976	161	681	90	294
Hf	2.27	5.71	2.87	2.78	3.04	3.05	3.08	2.41	2.59	5.02
Ta	1.14	3.74	1.96	2.00	1.94	0.98	2.13	0.97	1.73	3.71
Th	0.95	5.07	0.72	0.55	0.58	3.57	0.76	2.40	1.64	1.63
U	0.27	1.14	0.17	0.15	0.16	0.77	0.19	0.41	0.19	0.79

Table 1 (*continued*)

	Banfangqing									
Sample	BFQ-2	BFQ-3	BFQ-4	BFQ-5	BFQ-6	BFQ-7	BFQ-8	BFQ-9	BFQ-10	BFQ-11
Rock type	HT	HT	HT	HT	HT	LT	HT	LT	HT	HT
Height (m)										
Ba/Th	788	108	276	285	369	273	212	284	55	180
La/Nb	0.87	1.13	1.50	1.62	1.67	0.66	1.39	0.93	1.79	1.40
Th/Ta	0.83	1.36	0.37	0.28	0.30	3.63	0.36	2.48	0.95	0.44

Note: Ocp = Olivine clinopyroxenite, Cpx = Clinopyroxenite; Gb = Gabbro; Mt–Gb = Magnetite gabbro; HT = High-Ti basalt; LT = Low-Ti basalt; LOI = Loss on ignition; Major oxides are reported in weight percent (wt.%), and trace elements in parts per million (ppm).

SKLODG. Mass fractionation corrections for Sr and Nd isotopic ratios were based on values of $^{86}Sr/^{88}Sr = 0.1194$ and $^{146}Nd/^{144}Nd = 0.7219$. The $^{143}Nd/^{144}Nd$ ratios of the USGS standard rock BCR-2 determined during this study were 0.512 622 ± 0.000004(2σ). Rb–Sr and Sm–Nd isotopic compositions are listed in Table 2.

Platinum-group elements were analyzed by isotope dilution (ID)-ICP-MS at the SKLODG, using an improved technique reported by Qi et al. (2011). Ten grams of rock powder and appropriate amounts of the enriched isotope spike solution containing ^{193}Ir, ^{101}Ru, ^{194}Pt, and ^{105}Pd were carefully weighed and placed in a 120 ml PTFE beaker to remove silicates. After the beaker was sealed in a stainless steel pressure bomb, the dried residue was then digested with HF + HNO_3 at 190 °C for about 24 h. The eluted solution was evaporated to 2–3 ml and then transferred to a 15 ml centrifuging tube for ICP-MS measurement after chemical preparation. The average compositions of the five total procedural reagent blanks ranged from 0.008 ng (Ru) to 0.033 ng (Pd) and the detection limits ranged from 0.004 ng/g (Ir) to 0.014 ng/g (Pt). The concentrations of PGEs are given in Table 3.

5. Results

5.1. Major and trace element geochemistry

All of the analyzed samples are relatively fresh as observed under the microscope and as indicated by their small loss-on-ignition (LOI) values listed in Table 1, except for three gabbro samples

Table 2
Sr–Nd isotopes of the rocks and basalts of the Hongge intrusion.

Sample	Rock type	Rb	Sr	(87Sr/86Sr)m	(87Sr/86Sr)i	Sm	Nd	(143Nd/144Nd)m	(143Nd/144Nd)i	εNd(i)
HG0	Ocp	2.04	160	0.706195	0.706059	4.31	16.4	0.512521	0.511991	−2.3
HG6	Ocp	1.01	117	0.706056	0.705964	4.16	14.5	0.512539	0.511961	−1.9
HG18	Cpx	0.806	40.2	0.706288	0.706074	0.74	3.27	0.512514	0.512058	−2.4
HG19	Ocp	0.983	47.6	0.706343	0.706123	0.909	4.13	0.512500	0.512056	−2.7
HG25	Gb	39.5	1260	0.706602	0.706268	2.78	9.07	0.512583	0.511965	−1.1
HG28	Mt-Gb	0.419	55	0.705746	0.705665	2.36	8.41	0.512605	0.512040	−0.6
HG31	Mt-Gb	0.459	36.1	0.705787	0.705651	1.2	3.65	0.512615	0.511953	−0.4
BFQ-1	Basalt	5.64	520	0.705394	0.705278	5.92	27.9	0.512585	0.512157	−1.0
BFQ-4	Basalt	27.2	606	0.708726	0.708247	7.61	34.1	0.512386	0.511936	−4.9
BFQ-6	Basalt	74	673	0.708929	0.707756	7.39	32.3	0.512383	0.511922	−5.0
BFQ-8	Basalt	41.2	650	0.709105	0.708429	8.47	38.9	0.512342	0.511903	−5.8
BFQ-10	Basalt	33.4	603	/	/	5.86	24.1	0.512307	/	/
BFQ-11	Basalt	40.9	1080	0.706891	0.706487	10.3	53.9	0.512442	0.512057	−3.8
BC-1	Basalt	76.6	887	0.706963	0.706042	4.93	26.9	0.512421	0.512052	−4.2
BC-4	Basalt	44	810	0.707253	0.706673	22.6	153	0.512434	0.512136	−4.0

Note: Ocp = Olivine clinopyroxenite, Cpx = Clinopyroxenite; Gb = Gabbro; Mt–Gb = Fe–Ti oxide-bearing gabbro; HT = High-Ti basalt; LT = Low-Ti basalt.

Table 3
Whole rock platinum group element concentrations and the ratio of Pt ∗ 10^6/Y, Pd/Pt, Cu/Pd of the Hongge layered intrusion.

Rock type	STD	Ir (ng/g)	Ru (ng/g)	Rh (ng/g)	Pt (ng/g)	Pd (ng/g)	ΣPGE	Pt ∗ 10^6/Y	Pd/Pt	Cu/Pd
		16.178	11.336	100.000	2.227	2.588	132.329			
Ocp	HG0	0.344	0.885	0.127	2.592	0.687	4.635	2.04×10^5	0.265	5.08×10^4
Ocp	HG11	0.636	2.082	0.279	4.452	1.997	9.445	4.88×10^5	0.449	9.76×10^4
Cpx	HG14	0.152	0.676	0.025	0.820	0.591	2.265	5.99×10^4	0.721	4.16×10^5
Cpx	HG16	0.524	1.424	0.177	4.845	3.076	10.047	3.21×10^5	0.635	8.39×10^4
Mt-Cpx	HG18	0.173	2.127	0.125	2.617	2.026	7.068	1.24×10^6	0.774	3.21×10^4
Mt-Cpx	HG19	0.143	1.486	0.087	0.978	0.945	3.639	3.64×10^5	0.966	7.19×10^4
Cpx	HG22	0.018	0.241	0.017	0.553	0.462	1.290	9.12×10^4	0.835	2.53×10^5
Gab	HG24	0.077	0.173	0.057	1.166	1.236	2.708	4.32×10^4	1.060	4.89×10^4
Mt-Gb	HG25	0.008	0.424	0.012	0.045	0.140	0.630	3.98×10^3	3.144	1.41×10^5
Ore	HG31	0.024	0.375	0.032	0.372	0.383	1.186	9.99×10^4	1.030	3.67×10^5
LT	BC-1	0.008	0.387	0.005	0.036	0.075	0.511	1.60×10^3	2.058	9.01×10^5
HT	BFQ-1	0.100	0.361	0.084	1.196	0.598	2.340	6.26×10^4	0.500	8.72×10^4
HT	BFQ-4	0.006	0.175	0.014	0.128	0.321	0.643	4.87×10^3	2.511	9.92×10^4
HT	BFQ-6	0.006	0.131	0.019	0.050	0.278	0.484	1.97×10^3	5.519	1.17×10^5
HT	BFQ-8	0.005	0.136	0.018	0.108	0.478	0.744	3.68×10^3	4.442	6.55×10^4
HT	BFQ-10	0.008	0.137	0.018	0.161	0.453	0.776	7.12×10^3	2.815	4.20×10^4
HT	BFQ-11	0.014	0.191	0.012	0.196	0.537	0.951	6.52×10^3	2.745	8.19×10^4

Note: Ocp = Olivine clinopyroxenite; Cpx = Clinopyroxenite; Gb = Gabbro; Mt–Gb = Fe–Ti oxide-bearing gabbro; Mt-Cpx = Fe–Ti oxide-bearing clinopyroxenite; HT = High-Ti basalt; LT = Low-Ti basalt.

(HG21, HG24, HG26) in the upper zone. As expected from their range of modal mineralogy, the samples exhibit significant compositional variations. For example, SiO_2 contents range from 28.03 to 45.88 wt.% and Al_2O_3 contents from 3.10 to 11.59 wt.% (Table 1). Na_2O and K_2O range from 0.08 to 1.23 wt.% and from 0.01 to 1.26 wt.%, respectively, whereas CaO shows a range between 11.1 and 18.53 wt.%. For clinopyroxenite, there is a slight, periodic increase in TiO_2 and Fe_2O_3, ranging between 4.86 and 12.89 wt.% and 19.55 and 28.01 wt.%, respectively. However, the major oxide compositions do not show systematic variation, there exist a periodic slight increase in TiO_2 and Fe_2O_3 (as total iron) (Fig. 4). On the Harker diagrams (Fig. 4), the cumulate rocks show broad negative correlations between MgO and SiO_2, Al_2O_3, CaO and $Na_2O + K_2O$. Additionally, the TiO_2 and Fe_2O_3 contents of the clinopyroxenite are relatively high than the olivine-bearing clinopyroxenite (Fig. 4).

Whole-rock trace element data of mafic–ultramafic rocks and basalts are listed in Table 1. Chondrite-normalized REE patterns of all samples and Primitive mantle-normalized REE pattern of Banfangqing and Baicao basalts from the Hongge area are enriched in light REE (LREE) relative to heavy REE (HREE) with relative positive Eu anomalies and overall similar to ocean island basalts (OIB) (Fig. 5). Additionally, as shown in the primitive mantle-normalized trace element diagram, the olivine clinopyroxenite and clinopyroxenite samples have trace element patterns distinct from the Longzhoushan high-Ti basalts (LHTB), whereas the Banfangqing and Baicao basalts display similar pattern with LHTB. All samples also show a moderate negative Sr, Y, Zr–Hf anomaly and significant positive Ba, Nb–Ta anomaly (Fig. 5a, c, and e). V and Zr concentrations of the cumulate rocks range from 295 to 1160 ppm and 34 to 105 ppm, respectively. The Hongge magnetite ores have Ni contents ranging from 113 to 1030 ppm with an average of 535 ppm, much higher than Cu contents (20–221 ppm and 124 ppm on average, Table 1).

5.2. Platinum group elements (PGEs) and Cu, Cr

The concentrations and variation of PGEs and other chalcophile elements of representative rocks from the Hongge intrusion are listed in Table 3. Samples from the Hongge intrusion have higher PGE concentrations than the adjacent Baicao and Banfangqing flood basalts, even though the total PGE contents in all the studied samples are quite low (range from 0.511 to 10.047 ppb, Table 3). Cu concentrations vary between 20 and 258 ppm and are generally correlated with the modal abundance of sulfides. Cr concentrations vary between 42.5 and 3850 ppm which are resulted by the high Cr contents (>2360 ppm) massive ores located in the middle zone. One exception is a Fe–Ti oxide ore layer in the UGZ (sample

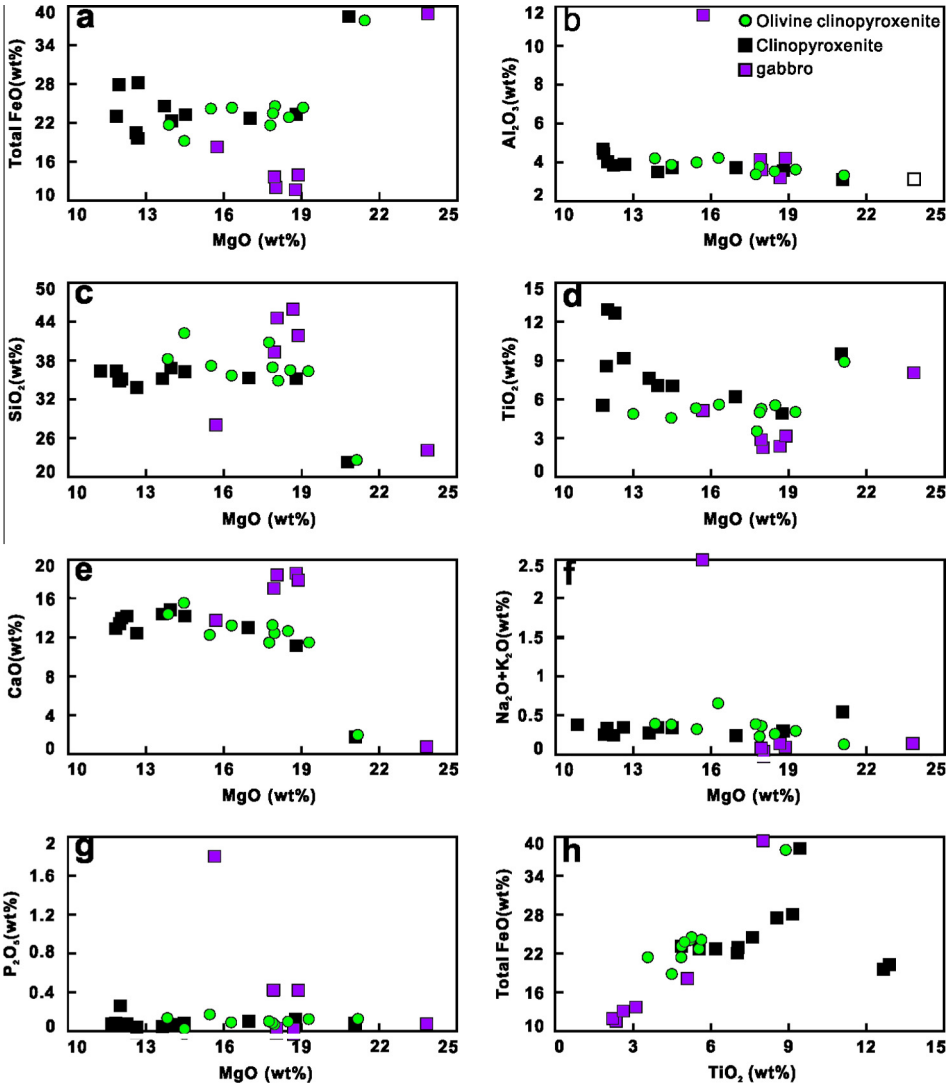

Fig. 4. Variations of Total FeO (a), Al_2O_3 (b), SiO_2 (c), TiO_2 (d), CaO (e), $Na_2O + K_2O$ (f), P_2O_5 (g) with MgO and Total FeO with TiO_2 (h) for different types of rocks from the Hongge intrusion, SW China.

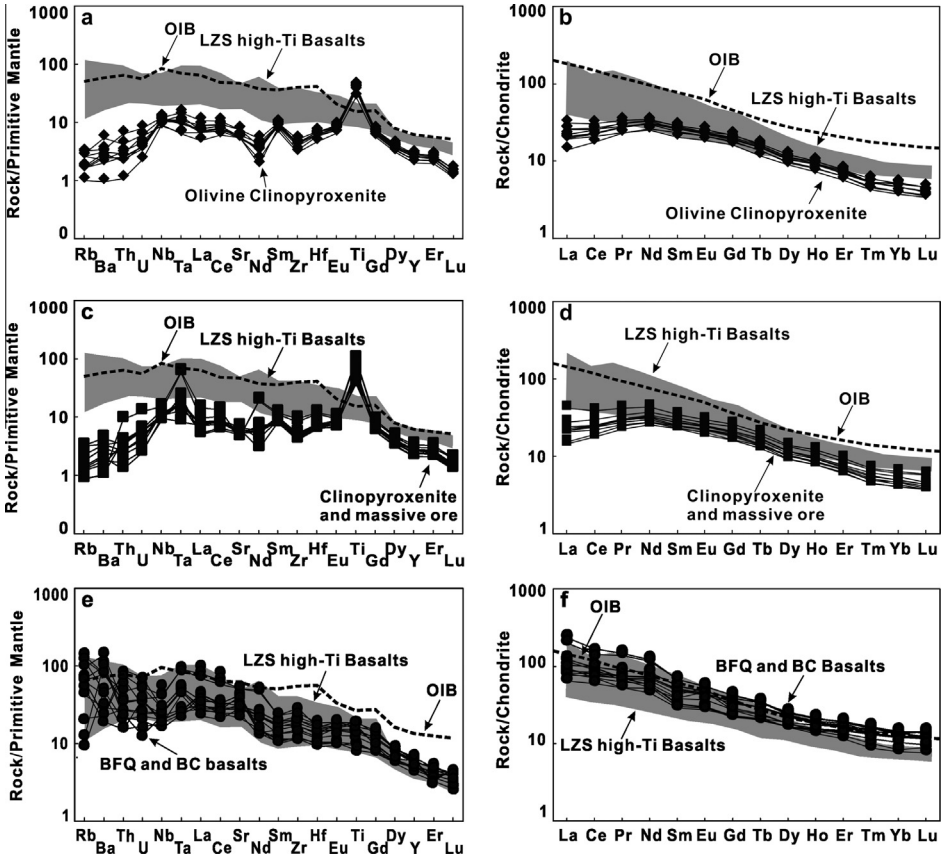

Fig. 5. (a), (c) and (f) Primitive-mantle normalized trace element diagrams of the Olivine-bearing clinopyroxenite, Fe–Ti oxide-bearing clinopyroxenite and Baicao as well as Banfangqing basalts from the Hongge intrusion. (b), (d) and (g): Chondrite-normalized REE patterns of the Olivine-bearing clinopyroxenite, Fe–Ti oxide-bearing clinopyroxenite and Baicao as well as Banfangqing basalts from the Hongge intrusion. Primitive-mantle normalizing values and average ocean-island basalt (OIB) pattern are from Sun and McDonough (1989). Data for the Longzhoushan basalts are from Qi et al. (2008).

HG-31), which has 82.3 ppm Cr. Cu/Pd ratios are variable for the studied samples, whereas the Cu/Pd values of the intrusive rocks are higher than that of the basalts (Fig. 11a).

The Hongge intrusive rocks and Banfangqing and Baicao basalts have distinct trends between Ir, Pd, Pt, and Rh on compositional correlation diagrams (Fig. 10). The Pd, Pt, and Rh contents of the Hongge samples decrease rapidly with decreasing Ir (Fig. 10a, b and c). Nearly all the PGE-depleted samples have Pd/Pt ratios higher than that of the primitive mantle (Pd/Pt = 0.6, Taylor and McLennan, 1985; Fig. 10d), except one sample (HG-0) in the lower zone. Additionally, the Banfangqing and Baicao basalts have lower Ir and Pt concentrations than the Hongge intrusive rocks and the Pd/Pt ratios in Fig. 10d indicate that there is an extensive decoupling between Pd and Pt.

5.3. Rb–Sr and Sm–Nd isotopes

The whole-rock Sr–Nd isotopic compositons of the rocks from the Hongge intrusion and Banfangqing and Baicao basalts are listed in Table 2. As shown in Fig. 8, the Hongge samples plot in the field of oceanic island basalt (OIB) and have much narrower ranges of εNd_{259Ma} and $(^{87}Sr/^{86}Sr)_{259Ma}$ values than the high-Ti Emeishan basalts. The calculated $\varepsilon Nd(i)$ and initial $^{87}Sr/^{86}Sr$ values (t = 259 Ma) of the Hongge intrusive rocks vary between −0.4 and −2.7, and between 0.7057 to 0.7063, respectively. Moreover, the basalts in this area display variable values of εNd_{259Ma} and $(^{87}Sr/^{86}Sr)_{259Ma}$, ranging from −1.0 to −5.8 and from 0.7053 to 0.7084, respectively. Samples from the Hongge intrusion are plotted between the coeval Panzhihua mafic intrusion in the Panxi area and the Emeishan low-Ti basalts (Fig. 8).

6. Discussion

6.1. Parental magma and fractional crystallization of the Hongge intrusion

One of the key factors in the modeling of the crystallization processes of an intrusion is the estimation of the composition of its parental magma(s) (Wager and Brown, 1968). As the chilled margins, dikes and sills are absent in Hongge, we failed to obtain the correct composition of parental liquid in traditional ways (Barnes et al., 2010; Cawthorn, 2006; Harmer and Sharpe, 1985). However, Bai et al. (2012a) using the MELTS program (Ghiorso and Sack, 1995) to simulate the fractional crystallization processes and shows that the Hongge parental magma probably contains 9.4 wt.% MgO and 14.5 wt.% FeOt. As the strong positive correlation between FeO and TiO_2 in Fig. 4h, the parental magma might also be riched in Ti. This can be further confirmed by the recent study (Bai et al., 2014) which indicated that the parental magma for Hongge Fe–Ti oxide deposit contains high Ti content (>3.5 wt.%). The magmas derived from primary mantle commonly have crystallized one or two mineral, more phases will appear with increasing degree of differentiation (Irvine, 1970). The cumulus assemblage of the Hongge intrusion contains at least four minerals (olivine + clinopyroxene + plagioclase + titanomagnetite), implying that the parental magma giving rise into the shallow magma chamber had already

undergone a certain degree of differentiation prior to emplacement. The cumulus assemblage above combined with the LREE riched compared to HREE (Fig. 5 b and d) imply the parental magma of Hongge was highly evolved.

The ore-forming processes of the Panzhihua and Baima intrusions in the Panxi area commonly related to the Fe and Ti riched magma replenishment from the deep magma chamber (Pang et al., 2009; Liu et al., 2014a). The two sharp geochemical breaks with respect to Fe–Ti oxide proportion (Mt/Ilm) and trace element ratios such as Ba/Th at the middle of the MCZ (Fig. 3f and i) indicating that the intrusion was recharged at least twice by more Fe and Ti-riched magma. This was further confirmed by the Harker diagrams (Fig. 4a and d) that the FeO and TiO_2 content of MCZ are higher than the LOZ. The relatively constant Fo values of olivine (Fig. 3c) and incompatible element (e.g., Zr and Y) from LOZ to UGZ (Fig. 3g and h) provide evidence that the Hongge magma chamber was continuously replenished by compositionally similar magmas. Trends of increasing SiO_2, CaO, FeO, TiO_2, Al_2O_3, $K_2O + Na_2O$ with decreasing MgO on the Harker diagrams (Fig. 4a–f) indicates that olivine, Fe–Ti oxides, clinopyroxene and plagioclase have fractionated during the solidification of magma. In addition, the TiO_2 and FeOt contents of clinopyroxenite in the MCZ are obviously higher than the olivine-bearing clinopyroxenite in the LOZ (Fig. 4a and d) combined with positive Ti anomalies of the clinopyroxenite and the olivine-bearing clinopyroxenite compared with Longzhoushan high-Ti basalts (Fig. 5a and c), which indicates that the magma replenishment provides a certain amount of Fe and Ti for Fe–Ti oxides saturation. The sharply decrease in TiO_2 and FeOt contents of gabbro (Fig. 3a and b) probably caused by abundant crystallization of magnetite and ilmenite. Based on the discussion above, we can speculate that the Fe and Ti riched parental magma for Hongge was highly evolved and magma replenishment occured in the shallow magma chamber.

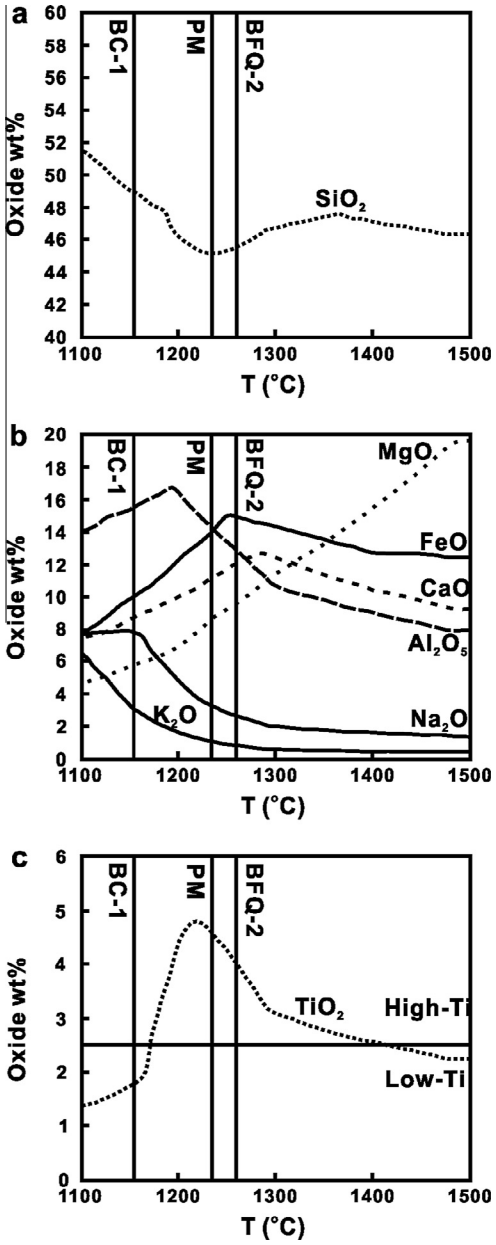

Fig. 6. Modeling results (a, b and c) of MELTS using a starting composition of melt inclusion (M8 62) of the high-Ti picrite (Kamenetsky et al., 2012), and assuming a pressure of 5000 bars, starting temperature of 1500 °C, ending temperature of 1100 °C, H_2O = 0.5 wt.%, FMQ. PM (Hongge parental magma) are after Bai et al. (2014). BC-1 and BFQ-2 are low-Ti and high-Ti basalts in Table 1.

Traditionally, incompatible element ratios are little influenced by the fractionation of most silicate phases, such as olivine and pyroxene. However, titanomagnetite and ilmenite are the dominant phases of accumulation in the Hongge intrusion, so we must check the influence of the fractionation of Fe–Ti oxides on the abundances and ratios of incompatible elements before we use them as a tracer. Although all rocks from the Hongge intrusion have primitive mantle-normalized incompatible element patterns similar to OIB, the difference can be observed that they exhibit both positive Ti anomalies and considerably variable Th, Ta and La (Fig. 5a, c and e), implying that a significant accumulation of Fe–Ti oxides in the Hongge intrusion has influenced some ratios of incompatible elements. In addition, the crudely decreasing Th/Ta and La/Nb with increasing TiO_2 (Fig. 7c and d) could be ascribed to accumulation of Fe–Ti oxide. Therefore, the crystallization of Fe–Ti oxide can influence the trace elements, especially the ratios of Zr, Nb, Hf or Ta to other HFSEs, although fractionation of clinopyroxene and minor phases can also control inter-element ratios. Moreover, the experiments of liquid crystallization by Thy et al. (2006) indicate that the P_2O_5/K_2O values increased by a factor of 1.3–1.5. In contrast, liquid immiscibility has a dramatic effect on the P_2O_5/K_2O ratio which in conjugate immiscible liquids may differ by one or two orders of magnitude (Watson, 1976; Dixon and Rutherford, 1979; Philpotts, 1982). Although Lindsley (2003) argued that immiscible Fe-liquid cannot be obtained by experiments, but the field evidence strong support the Fe–Ti oxide deposits of Chile appear to generate from Fe-rich immiscible liquid. In view that direct experimental demonstration of immiscibility is difficult and uncertain, we should also look for indirect and consequential evidence like, for example the variations of P_2O_5/K_2O ratio. However, for the Hongge intrusion, the P_2O_5/K_2O show constant variation that 0.53–4.36, 0.61–3.75 and 0.69–3.58 for the LOZ, MCZ and UGZ respectively (Fig. 3), excluding the abnormal samples (HG16, 22 and 26, in Table 1). Consequently, we argue that the constant P_2O_5/K_2O valus as shown in the stratigraphic column combined with the compatible behavior of HFSE indicates that massive ores in the Hongge intrusion were formed by crystallization and accumulation and does not favor the ore-formation mechanism of immiscible Fe-liquids (e.g. Zhou et al., 2005).

6.2. Genetic relation between the Hongge intrusion and the flood basalts

As a major part of the ELIP, flood basalts are coeval and spatially associated with numerous mafic–ultramafic intrusions (Zhong and Zhu, 2006; Zhou et al., 2002, 2008). Zhou et al. (2008) suggested that the Fe–Ti–V oxide deposits are genetically related to high-Ti basaltic magmas whereas the Cu–Ni–(PGE) sulfide-bearing

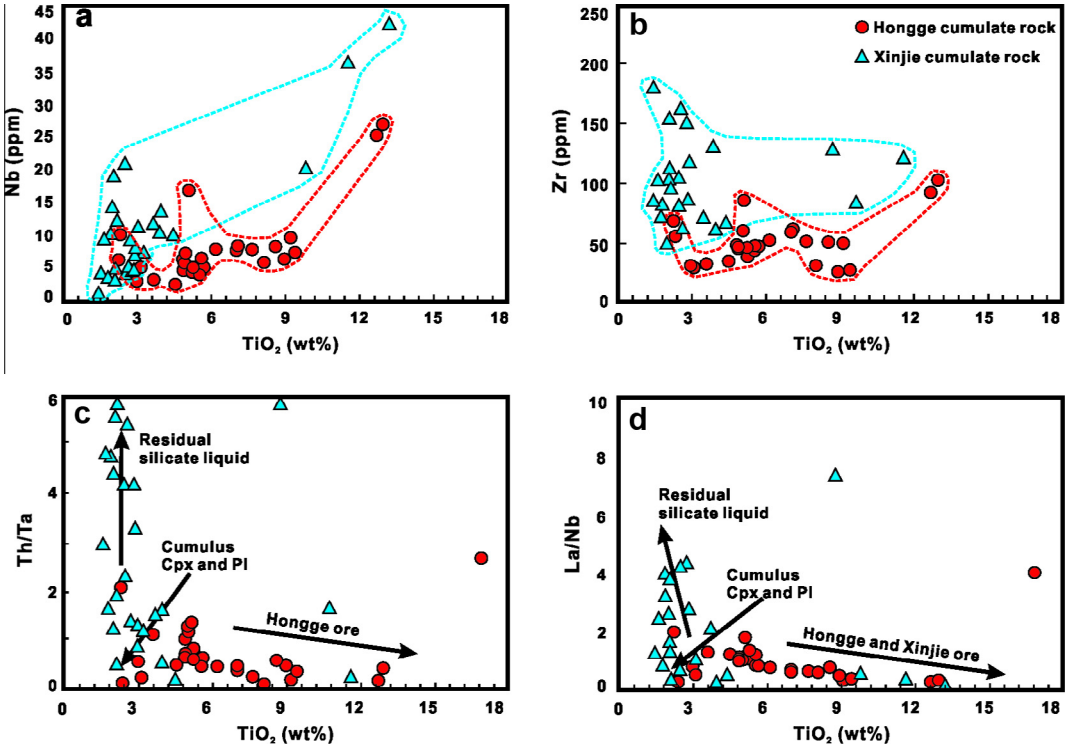

Fig. 7. Diagrams of TiO_2 vs. Nb, Zr, Th/Ta and La/Nb for the Hongge and Xinjie intrusions.

mafic–ultramafic intrusions were formed from low-Ti basaltic magmas. However, some researchers argued that the different types of mafic–ultramafic intrusions in the ELIP cannot simply be attributed to be genetically related special types of basalts, either high-Ti or low-Ti basalts (Hou et al., 2011; Zhang et al., 2009a; Hao et al., 2004). Here, the Banfangqing and Baicao basaltic lavas contain both low-Ti and high-Ti basalts near the Hongge Fe–Ti–V oxide deposits which offer an opportunity for us to explore the genetic relation between them.

Melt inclusion (M8 62, Kamenetsky et al., 2012) which contain 12.29 wt.% FeOt, 2.25 wt.% TiO_2, 19.68 wt.% MgO and 46.38 wt.% SiO_2 in olivine phenocrysts (Fo = 91.71) have been chosen to represent the primary magma composition for the MELTS modeling for the Baima and Hongge intrusions, respectively (Zhang et al., 2012; Luan et al., 2013). We also assumed the primary magma of the Hongge intrusion had a composition similar to the melt inclusion (M8 62) and employed the MELTS package (Ghiorso and Sack, 1995) to simulate the concealed crystallization path of the Hongge intrusion. We use a relatively low oxygen fugacity (fO_2 = FMQ), a starting temperature of 1300 °C, an ending temperature of 1100 °C, H_2O = 0.5 wt.% and pressure of 5000 bars (~15 km). The results of the MELTS modeling is shown in Fig. 6, at ~1260 °C and 1155 °C, the compositions of residual liquid are similar to our actual high-Ti (BFQ-2) and low-Ti (BC-1) basltic samples listed in this paper (Table 1) and can be produced from high-Ti and high-Mg picritic primary magma (M8 62). Hence, the Banfangqing high-Ti (BFQ-2) and Baicao low-Ti (BC-1) basalts seem to be derived from a common parental magma whereas different mantle sources. Besides, Bai et al. (2014) using the experimentally determined partition coefficient of 0.45 for TiO_2 between clinopyroxene and basaltic magma from Hauri et al. (1994) and the Fe–Mg exchange coefficient of 0.27 between clinopyroxene and melt from Bédard (2010) to figure out the concentrations of TiO_2 and the MgO/FeO ratios for the parental magma of the Hongge intrusion is estimated to be 3.9–4.9 and 0.63, respectively. However, MELTS calculations (Fig. 6b and c) indicates that when the temperature decreased to 1235 °C, the TiO_2 content and the MgO/FeO ratios of the residual liquid respectively increased to 4.58 and decreased to 0.62. Thus, the parental magma of the Hongge intrusion, the Banfangqing high-Ti(BFQ-2) and Baicao low-Ti(BC-1) basalts are the products of magma evolution from the same primamy magma and the evolving order can be observed in Fig. 6.

Zhong et al. (2005) provided comprehensive studies of the Hongge layered intrusion and suggested that it is contemporaneous and chemically correlated with Emeishan high-Ti basalts in the Pan–Xi area, southwestern China. However, more geochemical characteristics were discussed below to enhance our inferences above. First, the negative Sr anomalies and positive U, Th, Zr, and Hf anomalies in the Hongge rocks (Fig. 5) can be explained by upper crustal contamination because upper crustal rocks is typically enriched in these elements and depleted in Sr (Taylor and McLennan, 1985). Besides, as εNd(t) values are seldom affected by postmagmatic alteration, they are a useful tool to trace the magma sources in traditional. The samples of the Hongge plot near the Yangtze lower and middle crust (Fig. 8), it suggests that the crustal contamination probably occurred during the primitive magma transportation en rounting from the deep crust to the shallow magma chamber of the Hongge intrusion. Therefore, we can speculate that the variable εNd(t) values of the samples (Table 2) in the Hongge intrusion and lavas could be attributed to variable extent of crustal contamination. In addition, the whole rock Sr–Nd isotopic data of Hongge intrusive rocks, Banfangqing and Baicao basaltic rocks plotted in the region of Emeishan low-Ti basalts (Fig. 8) combined with they chemically resemble OIB (Fig. 5) indicate they are co-magmatic rather than derivation from a distinct source. In other words, the Hongge Fe–Ti–V oxide deposit is not genetically related to high-Ti or low-Ti basalts. Furthermore, the significant low MgO content (<9 wt.%) for all the high-Ti and low-Ti basalts in this paper (Table 1), indicating that they are the erupted residual melts that experienced variable degree of

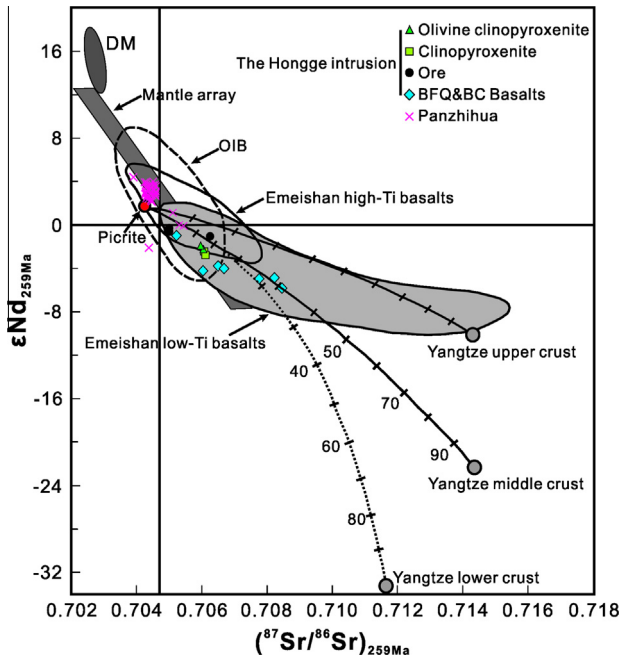

Fig. 8. Binary plots of εNd_{259Ma} vs.$(^{87}Sr/^{86}Sr)_{259Ma}$ for the rocks from the Hongge intrusion. The calculated parameters of Nd (ppm), εNd(t), Sr (ppm) and $(^{87}Sr/^{86}Sr)_i$ are 19, +2, 140 and 0.704, which are the average values from picrites in Lijiang as parental magmas (Zhang et al., 2006); 20, −10, 220, 0.715 and 20, −22, 220, 0.715, as well as 21, −33, 517, 0.712 as the average components of the Yangtze upper, middle and lower crusts respectively (Ma et al., 2000; Wang et al., 2007). The numbers indicate the percentages of participation of the crustal materials in theory, but not the actual percentages of crustal contamination, and these numbers are used for the aim of comparison. DM (depleted mantle) and mantle array are after Zindler and Hart (1986). Panzhihua data are after Zhou et al. (2008), Zhang et al. (2009b) and Song et al. (2013). Emeishan high-Ti and low-Ti basalts date are from Xu et al. (2001), Xiao et al. (2003, 2004a, 2004b), Zhou et al. (2006) and Song et al. (2008).

evolution. Conclusively, we speculate the Banfangqing and Baicao basalts, regardless of what the type, show no obvious genetic links to the Hongge ore-bearing intrusion of the ELIP and they are co-magmatic liquid with the parental magma of the Hongge intrusion.

6.3. Depletion of PGEs and sulfide segregation from S-undersaturated magma

Extremely low PGE contents (<0.1–3 ppm) in the bulk sulfides of the Hongge intrusion have been known for some times (Zhong et al., 2002). Bai et al. (2012b) argued that PGE depletion in the Hongge intrusion was probably due to sulfide saturation and segregation in deep level. However, the actually mechanism for the depletion of PGEs remain controversial. We make attempt to explore the nature of the primitive magma and decipher the meaning of PGE depletion for better understanding the magma evolution of the Hongge intrusion.

Fractionation of chromites and segregated sulfide would cause PGE depletion of basaltic magma, which may occur in both S-undersaturated or S-saturated conditions (Song et al., 2009). The discrimination between PGE depletion for S-saturated vs. S-undersaturated magmas can be constrained by using various trace elements and PGEs. Pd has a higher sulfide melt/silicate melt partition coefficient than Pt (Fleet and Stone, 1991; Peach et al., 1994; Vogel and Keays, 1997), the Pd/Pt ratio increase significantly from the typical mantle ratio of 0.6 (Taylor and McLennan, 1985) with the fractionation of mafic minerals implying that the magma has not been acheived S-saturation. In addition, the significant Ni and Cr depletion with the olivine and chromite fractionation also confirm the system is sulfide free.

The positive correlations of Cr and Ni with MgO and Cr with Ni (Fig. 9a–c) of the Hongge intrusive rocks, indicate that a large proportion of olivine and chromite fractionated from the primitive picritic magma at depth. The commonly high Pd/Pt ratio of the Banfangqing and Baicao basalts may suggest the PGE depletion occurring under S-undersaturated basaltic magma. Besides, Wang et al. (2008) and Zhou et al. (2008) suggested that the parental magma of mafic–ultramafic intrusions in Panxi area have genetic link with the Emeishan high-Ti basalt in composition, so the parental magma for the Hongge intrusion are probably S-undersaturated. The absence of any correlation between Ni and Cu (Fig. 9d) also support the depiction above. However, PGE are more compatible in sulfide liquid relative to Cu and Ni under the S-saturation condition, the former has extremely high partition coefficients between sulfide and silicate melt compare to the latter (Peach et al., 1990, 1994), which would lead a high Cu/Pd value in the residual magma (Barnes and Picard, 1993). The Cu/Pd values of the Hongge rocks range from 4.16×10^5 to 3.21×10^4 are lower than the sulfide-mineralized samples from the Limahe intrusion, which is considered to be related to second-stage sulfide segregation (Tao et al., 2008). In addition, the Cu/Pd values of Hongge intrusive rocks and basalts are commonly higher than those of the PGE undepleted Emeishan high-Ti basalts (Zhong and Zhu, 2006; Qi and Zhou, 2008; Song et al., 2009, Fig. 11a) and also are obviously higher than the Jinbaoshan Pt–Pd deposit in the central ELIP, which are considered to be formed from sulfide segregation (Tao et al., 2007, Fig. 11a). Maier and Barnes (1999) considered that the high Cu/Pd ratio of the residual melt is a feature of sulfide segregation, so we consider that the Hongge intrusion must have experienced sulfide segregation at depth, according to the strong depletion of PGEs and high Cu/Pd ratios. In addition, the correlation of Ir, Pd and Pt with Rh and the decoupling of Pd and Pt illustrated in Fig. 9, the sharp decrease in $Pt \times 10^6/Y$ ratios (Fig. 11b) indicate that the variations in PGE concentrations and low Pd/Pt ratios of the Hongge intrusive rocks were resulted from sulfide separation (Fig. 10). Lightfoot and Keays (2005) indicated that S-saturation and PGE-depletion has genetic link with extensive crustal contamination in the Siberian trap basalts and the reason is probably that crustal contamination can provide a source of S (Song et al., 2009). As the primitive magma of the Hongge intrusion experienced crustal contamination, it maybe the reason to drive the magma to S-saturation by the assimilation of the external S.

6.4. Implications for the formation of Fe–Ti–V ore of Hongge intrusion

Several layered mafic–ultramafic intrusions of the ELIP host large Fe–Ti–V oxide deposits reserve about ten billion tons of iron and titanium oxide ores in the Panxi region, SW China and have been a focus of recent studies about magmatic evolution and its metallogenesis (Pang et al., 2010; Song et al., 2013; Wang and Zhou, 2013; Zhang et al., 2009b; Zhong and Zhu, 2006; Zhong et al., 2003, 2004, 2005; Zhou et al., 2005, 2008, 2013). Two main ore-forming mechanisms have been proposed for the Panzhihua intrusion which is a typical layered mafic intrusion and attracts majority of previous studies in the Panxi area: (a) early crystallization of Fe–Ti oxides from a Fe and Ti riched parent magma and oxides accumulation through crystal settling at the base of the intrusion (Pang et al., 2008a, 2008b; Shellnutt and Pang, 2012), and (b) density Fe-rich immiscible liquid from a ferrogabbroic parent magma (Liu et al., 2014a). Nevertheless, the precise mechanisms by which millions of tonnes of Fe, Cr, Ti and V become concentration in this area remain poorly known.

Howarth et al. (2013a) demonstrated the massive Fe–Ti oxide ore layers of the Panzhihua intrusion were contributed to multiple

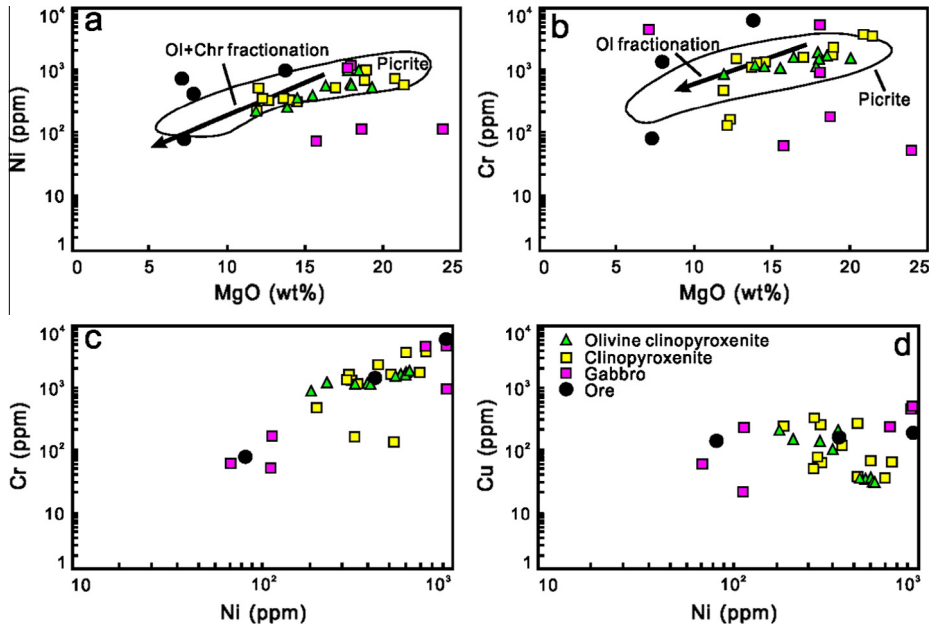

Fig. 9. Whole-rock geochemical variation diagrams for the Olivine-bearing Clinopyroxenite, Clinopyroxenite, Gabbro and Fe–Ti oxides of the Hongge intrusion. (a) Ni vs. MgO showing good correlation with picrites evolution. (b) Cr vs. MgO showing correlation of Cr with MgO. (c) Cr vs. Ni showing correlation. (d) Cu vs. Ni showing no correlation. Picrite field in a and b is after Li et al. (2012).

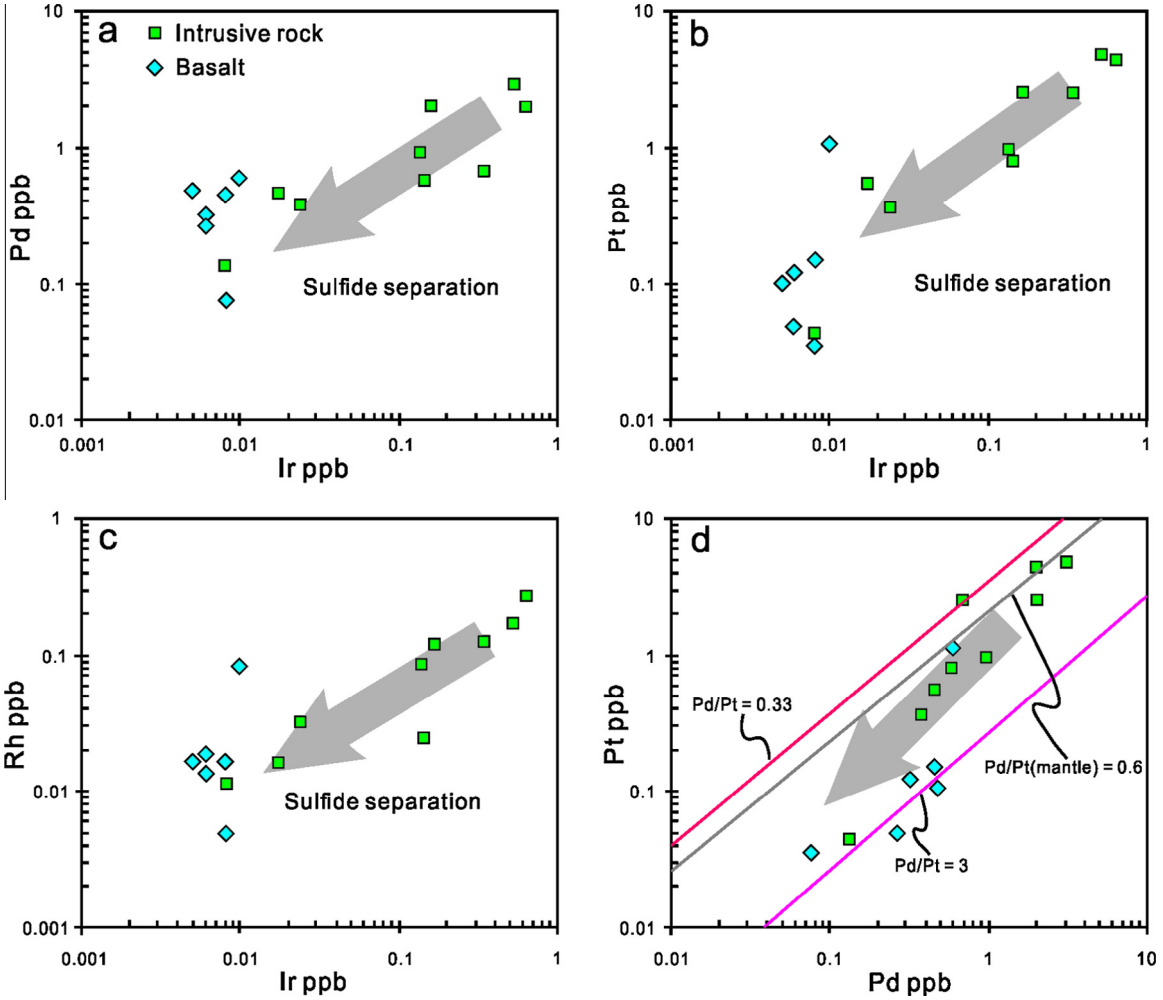

Fig. 10. Correlations between PGE. As Ir decreases, Pd, whole Pt and Rh of the intrusive rock and basalts decreases (a, b and c). Decoupling of Pt and Pd of the intrusive rocks and basalts of Hongge intrusion is displayed by the diagram of Pt vs. Pd (d).

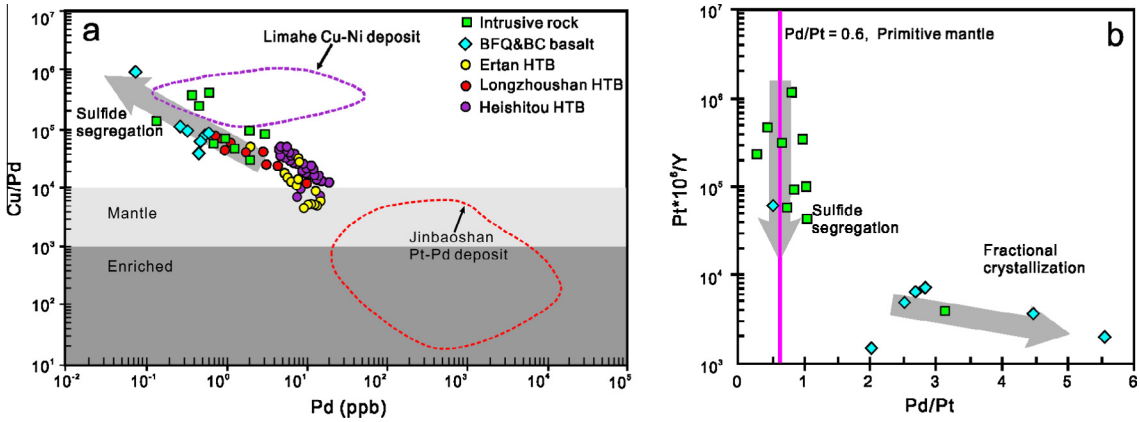

Fig. 11. Plots of Cu/Pd vs. Pd (a) and Pt $*$ 10^6/Y vs. Pd/Pt (b), showing that intrusive rocks and basalts of the Hongge intrusion resulted from segregation of sulfides. Range of Cu/Pd ratio of the primitive mantle are from Taylor and McLennan (1985) and Maier and Barnes (1999). HTB = High-Ti Basalt.

replenishments of Fe and Ti riched magma with variable H_2O contents in an open magma chamber. However, Luan et al. (2013) argued that the external H_2O intruded into the parental magma of the Hongge intrusion during the assimilation of the footwall meta-sandstone resulted in early crystallization of Fe–Ti oxides. It is possible that there is genetic link relationship between the intruding H_2O and extensive crystallization of Fe–Ti oxides, which probably was the key factor for us to better understand the magmatic evolution and metallogenesis of the Hongge intrusion.

The study of Sobolev and Chaussidon (1996) indicate that H_2O content of mantle derived magmas is usually less than 0.51 wt.%. In addition, as the roof rocks of the Hongge intrusion are basalts and syenites which are unlikely to contain significant H_2O and the carbonates are absent in the Hongge area (Fig. 1), so we presumed the parental magma arrived at the Hongge intrusion are anhydrous magma. Howarth and Prevec (2013) demonstrated that magmas with low H_2O generally followed the typical Fenner Fe-enrichment, therefore we presumed that the anhydrous parental magma came into the Hongge shallow magma chamber which followed the Fenner trend and began to crystallise olivine, clinopyroxene and minor Fe–Ti oxides to form the Fe–Ti oxide free cumulate rocks at the base of the intrusion, and the magma was gradually riched in Fe which are preparing for the onset of Ti-magnetita crystallization on the top of the LOZ and the bottom of the MCZ. The increased anorthite contents in plagioclase could be resulted by external H_2O joined in the basaltic magma (Sisson and Grove, 1993; Koepke et al., 2005). However, the chemical data of the plagioclase for the Hongge intrusion (Bai, 2012) shown that the average An of plagioclase increased from 62.68 (MCZ) to 74.63 (UGZ). Besides, the samples of Luan et al. (2013) colleted from the drill cores from the south part of the Hongge intrusion indicated that the UGZ is characterized by abundance of apatite gabbro, which contains 3–5% hornblende (locally up to 10%). In addition, the mineral proportion of hornblende in the MCZ about 3–12%

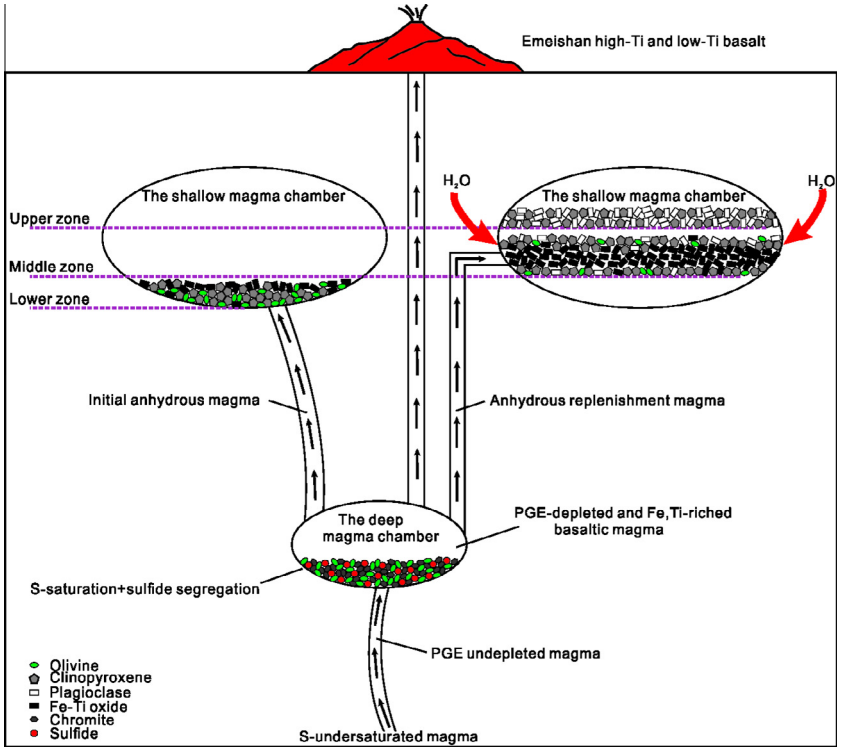

Fig. 12. A petrogenetic model showing the formation of the Hongge intrusion, SW China.

was calculated through the reflectd light microscope images (Fig. 2c and d), imply that the hornblende is the essential mineral in the Hongge MCZ and accumulation of Fe–Ti oxides was effected by the intruded water more or less. Moreover, the reaction rim of olivine in the massive ore (Fig. 2e) also indicate that the system was hydrous during extensive crystallization of Fe–Ti oxides. Recent experimental work of Gaillard et al. (2001) indicated that dissolved water has a specific positive effect on the Fe^{3+}/Fe^{2+} ratio of the silicic magma when fO_2 < FMQ + 1.7. Our unpublished calculated results of oxygen fugacities for the LOZ (FMQ-1.29 to FMQ-0.2) and MCZ (FMQ-0.49 to FMQ + 0.82)combined with the increased Fe^{3+}/Fe^{2+} ratio (Fig. 3e) in the MCZ of the Hongge intrusion inspired us to speculate that there is external H_2O intruded into the shallow chamber during formation of the MCZ. Therefore, we presume that the multiple replenishment magma injection into the Hongge intrusion combined with the residual liquid heating of strata around the magma chamber and absorbing the H_2O within it, which formed a water circulation system to supply the H_2O for extensive crystallization and acumulation of Fe–Ti oxides. It may be reasonable to suggest that silicate minerals would crystallized from low-H_2O magma in the early stage to form the lower zone of the intrusion, whereas plenty of Fe–Ti oxide crystallization appeared in the later stage due to heating of strata which changes the magma system into H_2O-rich (Fig. 12).

In summary, the primitive magma originate from the S-undersaturated magma system initially, then crustal contamination event occured during the parent magma transport from the crust source to the current shallow magma chamber provide crustal S to change the S-undersaturated magma into S-saturated. Subsequently, sulfide segregation promote the parent magma for Hongge strong PGEs depletion occured in the deep magma chamber (Fig. 12). The anhydrous or containing little water parental magma evolving at depth intrude into the shallow magma chamber of the Hongge intrusion which followed by normal fractional crystallization path to crystallize olivine, clinopyroxene, minor magnetite and ilmenite under the relatively "closed" system to form the lower zone of the Hongge intrusion. Crystallization of these minerals lead to the residual magma gradually enriching in FeOt and TiO_2, the injected magma and the initial hydrous magma together heating the strata to produce H_2O and the replenishment of the new Fe and Ti-riched magma, the three factors above may account for extensive crystallization and acumulation of Fe–Ti oxides to form the thick ore layers in the middle zone of the Hongge intrusion.

7. Conclusions

The magma evolving processes of the Hongge intrusion includes three stages. In the first stage, S-undersaturated and PGE-undepleted magma which undergo a certain degree of crustal contamination to make the magma system S-saturation, and then crystallized olivine, chromite and sulfide in the deep magma chamber. The residual PGE-depleted and Fe, Ti-riched arrived at the shallow magma chamber to crystallize olivine, clinopyroxene, minor magnetite and ilmenite consist of the lower part of the Hongge intrusion. The massive Fe–Ti oxide layers in the middle zone of the Hongge intrusion are closely related to the event that new replenishment magma mixing with the former residual Fe, Ti-riched liquid which heating the strata to attract H_2O.

Acknowledgements

This study was supported by the National 973 Program of China (2012CB416804 and 2014CB440906), CAS/SAFEA International Partnership Program for Creative Research Teams (KZZD-EW-TZ-20), and National Natural Sciences Foundations of China (41473051) to Tao yan. We acknowledge Yin yi-fan and Xiao fang for the PGE and Sr–Nd isotope analysis. Ms. Hu jing and Huang Yan are thanked for their efforts in trace element analysis.

References

Bai, Z.J., 2012. Petrogenesis and Fe–Ti Oxide Mineralization of the Mafic–untramafic Layered Intrusions in the Pan–Xi Area, SW China – A Case Study of the Hongge and Panzhihua Layered Intrusion (Thesis in Chinese).

Bai, Z.J., Zhong, H., Li, C.S., Zhu, W.G., Xu, G.W., 2012a. Platinum-group elements in the oxide layers of the Hongge mafic–ultramafic intrusion, Emeishan Large Igneous Province, SW China. Ore Geol. Rev. 46, 149–161.

Bai, Z.J., Zhong, H., Naldrett, A.J., Zhu, W.G., Xu, G.W., 2012b. Whole-rock and mineral composition constraints on the genesis of the giant hongge Fe–Ti–V oxide deposit in the Emeishan Large Igneous Province, Southwest China. Econ. Geol. 107, 507–524.

Bai, Z.J., Zhong, H., Li, C.S., Zhu, W.G., He, D.F., Qi, L., 2014. Contrasting parental magma compositions for the Hongge and Panzhihua magmatic Fe–Ti–V oxide deposits, Emeishan large igneous province, SW China. Econ. Geol. 109, 1763–1785.

Barnes, S.J., Picard, C.P., 1993. The behavior of platinum-group elements during partial melting, crystal fractionation, and sulphide segregation: an example from the Cape Smith Fold Belt, northern Quebec. Geochim. Cosmochim. Acta 57, 79–87.

Barnes, S.J., Naldrett, A.J., Gorton, M.P., 1985. The origin of the fractionation of platinum-group elements in terrestrial magmas. Chem. Geol. 53, 303–323.

Barnes, S.J., Maier, W.D., Curl, E.A., 2010. Composition of the marginal rocks and sills of the Rustenburg Layered Suite, Bushveld Complex, South Africa: implications for the formation of the Platinum-Group Element Deposits. Econ. Geol. 105, 1491–1511.

Bédard, J.H., 2010. Parameterization of the Fe–Mg exchange coefficient (Kd) between clinopyroxene and silicate melts. Chem. Geol. 274, 169–176.

Cabri, L.J., 2002. The geology, geochemistry, mineralogy, mineral beneficiation of the platinum-group elements. Can. Inst. Min. Metall. Petrol. 54, 852.

Cawthorn, R.G., 2006. Cr and Sr: keys to parental magmas and processes in the Bushveld Complex, South Africa. Lithos 95, 381–398.

Chung, S.L., Jahn, B.M., 1995. Plume–lithosphere interaction in generation of the Emeishan flood basalts at the Permian–Triassic boundary. Geology 23, 889–892.

Dixon, S., Rutherford, M.J., 1979. Plagiogranites as late-stage immiscible liquids in ophiolite and mid-ocean ridge suites: an experimental study. Earth Planet. Sci. Lett. 45, 45–60.

Dong, S.Y., Zhang, Z.C., 2009. Geochemical behavior of yttrium in Fe–Ti oxides – an example inferred from the Emeishan large igneous province. Geol. Rev. 50, 355–360 (in Chinese with English abstract).

Fleet, E.M., Stone, W.E., 1991. Partitioning of platinum-group elements in the Fe–Ni–S system and their fractionation in nature. Geochim. Cosmochim. Acta 55, 245–253.

Gaillard, F., Scaillet, B., Pichavant, M., Beny, J.M., 2001. The effect of water and fO_2 on the ferric–ferrous ratio of silicic melts. Chem. Geol. 174, 255–273.

Ganino, C., Arndt, N.T., Zhou, M.-F., Gaillard, F., Chauvel, C., 2008. Interaction of magma with sedimentary wall rock and magnetite ore genesis in the Panzhihua mafic intrusion, SW China. Miner. Deposita 43, 677–694.

Ghiorso, M.S., Sack, R.O., 1995. Chemical mass transfer in magmatic processes IV. A revised and internally consistent thermodynamic model for the interpolation and extrapolation of liquid–solid equilibria in magmatic systems at elevated temperatures and pressures. Contrib. Miner. Petrol. 119, 197–212.

Guo, F., Fan, W.M., Wang, Y.J., Li, C.W., 2004. When did the Emeishan mantle plume activity start? Geochronological and geochemical evidence from ultramafic–mafic dikes in southwestern China. Int. Geol. Rev. 46, 226–234.

Hao, Y., Zhang, Z., Wang, F., Mahoney, J.J., 2004. Pereogenesis of high-Ti and low-Ti basalts from the Emeishan large igneous province. Geol. Rev. 50, 587–592 (in Chinese with English abstract).

Harmer, R.E., Sharpe, M.R., 1985. Field relations and strontium isotope systematic of the marginal rocks of the eastern Bushveld Complex. Econ. Geol. 80, 813–837.

Hauri, E.H., Wagner, T.P., Grove, T.L., 1994. Experimental and natural partitioning of Th, U, Pb and other trace elements between garnet, clinopyroxene and basaltic melts. Chem. Geol. 117, 149–166.

He, Q., Xiao, L., Balta, B., Gao, R., Chen, J., 2010. Variety and complexity of the Late-Permian Emeishan basalts: reappraisal of plume–lithosphere interaction processes. Lithos 119, 91–107.

Hou, T., Zhang, Z.C., Kusky, T., Du, Yangsong, Liu, junlai, Zhao, Zhidan, 2011. A reappraisal of the high-Ti and low-Ti classification of basalts and petrogenetic linkage between basalts and mafic–ultramafic intrusions in the Emeishan Large Igneous Province, SW China. Ore Geol. Rev. 41, 133–143.

Howarth, G.H., Prevec, S.A., 2013. Hydration vs. oxidation: modelling implications for Fe–Ti oxide crystallisation in mafic intrusions, with specific reference to the Panzhihua intrusion, SW China. Geosci. Front. 4, 555–569.

Howarth, G.H., Prevec, S.A., Zhou, M.-F., 2013. Timing of Ti-magnetite crystallisation and silicate disequilibrium in the Panzhihua mafic layered intrusion: implications for ore-forming processes. Lithos 170–171, 73–89.

Irvine, T.N., 1970. Crystallization Sequences in the Muskox Intrusion and other Layered Intrusions. 1. Olivine–pyroxene–Plagioclase Relations. The Geological Society of South Africa, Special Publications, pp. 441–476.

Irvine, T.N., 1975. Crystallization sequences in Muskox intrusion and other layered intrusions. 2. Origin of chromitite layers and similar deposits of other magmatic ores. Geochim. Cosmochim. Acta 39, 991–1020.
Kamenetsky, V.S., Chung, S.L., Kamenetsky, M.B., Kuzmin, D.V., 2012. Picrits from the Emeishan large igneous province, SW China: a compositional continuum in primitive magmas and their respective mantle sources. J. Petrol. 53, 2095–2113.
Keays, R.R., 1995. The role of komatiitic and picritic magmatism and S-saturation in the formation of ore deposits. Lithos 34, 1–18.
Keays, R.R., Lesher, C.M., Lightfoot, P.C., Farrow, C.E.G., 1999. Dynamic processes in magmatic ore deposits and their application in mineral exploration. Geol. Assoc. Canada, Short Course Volume 13, 477.
Koepke, J., Feig, S.T., Snow, J., 2005. Late-stage magmatic evolution of oceanic gabbros as a result of hydrous partial melting: evidence from the ODP Leg 153 drilling at the Mid-AtlanticRidge. Geochem. Geophys. Geosyst. 6, 1–27.
Li, C., Tao, Y., Qi, L., Ripley, E.M., 2012. Controls on PGE fractionation in the Emeishan picrites and basalts: constraints from integrated lithophile–siderophile elements and Sr–Nd isotopes. Geochim. Cosmochim. Acta 90, 12–32.
Liang, Y.B., Liu, T.Y., Song, G.R., Jin, Z.M., 1998. Platinum Group Element Deposits in China. Metallurgical Industry Press, Beijing (in Chinese).
Lightfoot, P.C., Keays, R.R., 2005. Siderophile and chalcophile metal variations in flood basalts from the Siberian Trap, Noril'sk region: implication for the origin of the Ni–Cu–PGE sulfide ores. Econ. Geol. 100, 439–462.
Lindsley, 2003. Do Fe–Ti Oxide Magmas Exist? Geology: Yes; Experiment: No! Ilmenite Deposits and their Geological Environment. Special Publishment-9, p. 34.
Liu, P.P., Zhou, M.F., Wang, C.Y., Xing, C.M., Gao, J.F., 2014a. Open magma chamber processes in the formation of the Permian Baima mafic–untramafic layered intrusion, SW China. Lithos 184–187, 194–208.
Liu, P.P., Zhou, M.F., Luais, B., Cividini, D., Rollion-Bard, C., 2014b. Disequilibrium iron isotopic fraction during the high-temperature magmatic differentiation of the Baima Fe–Ti oxide-ore bearing mafic intrusion, SW China. Earth Planet. Sci. Lett. 399, 21–29.
Lorand, J.P., Luguet, A., Alard, O., 2008. Platinum-group elements: a new set of key tracers for the Earth's interior. Elements 4, 247–252.
Luan, Y., Song, X.Y., Chen, L.M., Zheng, W.Q., Zhang, X.Q., 2013. Key factors controlling the accumulation of the Fe–Ti oxides in the Hongge layered intrusion in the Emeishan Large Igneous Province, SW China. Ore Geol. Rev. 57, 518–538.
Ma, C., Ehlers, C., Xu, C., Li, Z., Yang, K., 2000. The roots of the Dabieshan ultrahigh-pressure metamorphic terrane: constraints from geochemistry and Nd–Sr isotope systematics. Precambr. Res. 102, 279–301.
Maier, M.D., Barnes, S.J., 1999. Platinum-group elements in silicate rocks of the lower, critical and main zones at Union Section, western Bushveld Complex. J. Petrol. 40, 1647–1671.
Pang, K.N., Li, C.S., Zhou, M.F., Ripley, E.M., 2008a. Abundant Fe–Ti oxide inclusions in olivine from the Panzhihua and Hongge layered intrusions, SW China: evidence for early saturation of Fe–Ti oxides in ferrobasaltic magma. Contrib. Miner. Petrol. 156, 307–321.
Pang, K.N., Zhou, M.F., Lindsley, D., Zhao, D.G., Malpas, J., 2008b. Origin of Fe–Ti oxide ores in mafic intrusions: evidence from the Panzhihua intrusion, SW China. J. Petrol. 49, 295–313.
Pang, K.N., Li, C.S., Zhou, M.F., Ripley, E.M., 2009. Mineral compositional constraints on petrogenesis and oxide ore genesis of the late Permian Panzhihua layered gabbroic intrusion, SW China. Lithos 110, 199–214.
Pang, K.N., Zhou, M.F., Qi, L., Shellnutt, J.G., Wang, C.Y., Zhao, G., 2010. Flood basalt-related Fe–Ti oxide deposits in the Emeishan large igneous province, SW China. Lithos 119, 123–136.
Peach, C.L., Mathez, E.A., Keays, R.R., 1990. Sulfide melt-silicate melt distribution coefficients for noble metals and other chalcophile elements reduced from MORB: implications for partial melting. Geochim. Cosmochim. Acta 54, 3379–3389.
Peach, C.L., Mathez, E.A., Keays, R.R., Reeves, S.J., 1994. Experimental determinated sulfide melt-silicate melt partition coefficients for iridium and palladium. Chem. Geol. 117, 361–377.
Philpotts, A.R., 1982. Compositions of immiscible liquids in volcanic rocks. Contrib. Miner. Petrol. 80, 201–218.
PXGT, 1987. Metallogenetic Conditions and Geologic Characters of the Hongge Vanadic Titanomagnetite Deposit, Sichuan. Geological Publishing House, Beijing, pp. 220 (in Chinese).
Qi, L., Zhou, M.F., 2008. Platinum-group elemental and Sr–Nd–Os isotopic geochemistry of Permian Emeishan flood basalts in Guizhou Province, SW China. Chem. Geol. 248, 83–103.
Qi, L., Hu, J., Gregoire, D.C., 2000. Determination of trace elements in granites by inductively coupled plasma mass spectrometry. Talanta 51, 507–513.
Qi, L., Wang, C.Y., Zhou, M.F., 2008. Controls on the PGE distribution of Permian Emeishan alkaline and peralkaline volcanic rocks in Longzhoushan, Sichuan Province, SW China. Lithos 106, 222–236.
Qi, L., Gao, J., Huang, X., Hu, J., Zhou, M.F., Zhong, H., 2011. An improved digestion technique for determination of platinum group elements in geological samples. J. Anal. At. Spectrom. 26, 1900–1994.
Shellnutt, J.G., 2014. The Emeishan large igneous province: a synthesis. Geosci. Front. 5, 369–394.
Shellnutt, J.G., Jahn, B.M., 2010. Formation of the Late Permian Panzhihua plutonic-hypabyssal-volcanic igneous complex: imolications for the genesis of Fe–Ti oxide deposits and A-type granites of SW China. Earth Planet. Sci. Lett. 289, 509–519.
Shellnutt, J.G., Jahn, B.M., 2011. Origin of Late Permian Emeishan basaltic rocks from the Panxi region (SW China): implications for the Ti-classification and spatial–compositional distribution of the Emeishan basalts. J. Volcanol. Geoth. Res. 199, 85–95.
Shellnutt, J.G., Pang, K.N., 2012. Mineral compositions of the Late Permian Baima layered gabbroic intrusion: constrains on petrogenesis. Mineral. Petrol. 106, 75–88.
Shellnutt, J.G., Zhou, M.F., Zellmer, G., 2009. The role of Fe–Ti oxide crystallization in the formation of A-type granitoids with implications for the Daly gap: an example from the Permian Baima igneous complex, SW China. Chem. Geol. 259, 204–217.
Shellnutt, J.G., Wang, K.L., Zellmer, G.F., Iizuka, Y., Jahn, B.M., Pang, K.N., Qi, L., Zhou, M.F., 2011. Three Fe–Ti oxide ore-bearing gabbro-granitoid complexes in the Panxi region of the Emeishan large igneous province, SW China. Am. J. Sci. 311, 773–812.
Shellnutt, J.G., Ma, G., Qi, L., 2013. Platinum-group elemental chemistry of the Baima and Taihe Fe–Ti oxide bearing gabbroic intrusions of the Emeishan Large Igneous Province, SW China. Chem. Erde-Geochem.
Sisson, T.W., Grove, T.L., 1993. Temperatures and H_2O contents of low-MgO high-alumina basalts. Contrib. Miner. Petrol. 113, 167–184.
Sobolev, A.V., Chaussidon, M., 1996. H_2O concentrations in primary melts from suprasubduction zones and mid-ocean ridges: implications for H_2O storage and recycling in the mantle. Earth and Planet. Sc. Lett. 137, 45–55.
Song, X.Y., Zhou, M.F., Hou, Z.Q., Cao, Z.M., Wang, Y.L., Li, Y.G., 2001. Geochemical constraints on the mantle source of the upper Permian Emeishan continental flood basalts, southwestern China. Int. Geol. Rev. 43, 213–225.
Song, X.Y., Zhou, M.F., Cao, Z.M., Sun, M., Wang, Y.L., 2003. Ni–Cu–(PGE) magmatic sulfide deposits in the Yangliuping area, Permian Emeishan Igneous Province, SW China. Miner. Deposita 38, 831–843.
Song, X.Y., Qi, H.W., Robinson, P.T., Zhou, M.F., Cao, Z.M., Chen, L.M., 2008. Melting of the subcontinental lithospheric mantle by the Emeishan mantle plume; evidence from the basal alkaline basalts in Dongchuan, Yunnan, Southwestern China. Lithos 100, 93–111.
Song, X.Y., Keays, R.R., Xiao, L., Qi, H.W., Ihlenfeld, C., 2009. Platinum-group element geochemistry of the continental flood basalts in the central Emeishan Large Igneous Province, SW China. Chem. Geol. 262, 246–261.
Song, X.Y., Qi, H.W., Hu, R.Z., Chen, L.M., Yu, S.Y., Zhang, J.F., 2013. Formation of thick stratiform Fe–Ti oxide layers in layered intrusion and frequent replenishment of fractionated mafic magma: evidence from the Panzhihua intrusion, SW China. Geochem. Geophys. Geosyst. 14, 712–732.
Sun, S.S., McDonough, W.F., 1989. Chemical and isotopic systematics of oceanic basalts: implications for mantle composition and processes. In: Saunders, A.D., Norry, M.J. (Eds.), Magmatism in the Ocean Basin, vol. 42. Geological Society Specical Publication, pp. 313–345.
Tao, Y., Li, C.S., Hu, R.Z., Ripley, E.M., Du, A.D., Zhong, H., 2007. Petrogenesis of the Pt–Pd mineralized Jinbaoshan ultramafic intrusion in the Permian Emeishan Large Igneous Province, SW China. Contrib. Miner. Petrol. 153, 321–337.
Tao, Y., Li, C.S., Song, X.Y., Ripley, E.M., 2008. Mineralogical, petrological, and geochemical studies of the Limahe mafic–ultramatic intrusion and associated Ni–Cu sulfide ores, SW China. Miner. Deposita 43, 849–872.
Tao, Y., Ma, Y.S., Miao, L.C., Zhu, F.L., 2009. SHRIMP U–Pb zircon age of the Jinbaoshan ultramafic intrusion, Yunnan Province, SW China. Chin. Sci. Bull. 54, 168–172.
Taylor, S.R., McLennan, S.M., 1985. The Continental Crust: Its Composition and Evolution: London. Blackwell Scientific Publications, UK, p. 312.
Thy, P., Lesher, C.E., Nielsen, T.F.D., Brooks, C.K., 2006. Experimental constraints on the Skaergaard liquid line of descent. Lithos 92, 154–180.
Vogel, D.C., Keays, R.R., 1997. The application of platinum group geochemisty in constraining the source of Basalt Magmas: results from the Newer Volcanic Province, Victoria, Australia. Chem. Geol. 136, 181–204.
Wager, L.R., Brown, G.M., 1968. Layered Igneous Rock. Oliver & Boyd, Edinburgh, p. 588.
Wang, C.Y., Zhou, M.F., 2013. New textural and mineralogical constraints on the origin of the Hongge Fe–Ti–V oxide deposit, SW China. Miner. Deposita 48, 787–798.
Wang, C.Y., Zhou, M.F., Keays, R.R., 2006. Geochemical constraints on the origin of the Permian Baimazhai mafic–ultramafic intrusion, SW China. Contrib. Miner. Petrol. 152, 309–321.
Wang, C.Y., Zhou, M.F., Qi, L., 2007. Permian flood basalts and mafic intrusions in the Jinping (SW China)-Song Da (northern Vietnam) district: mantle sources, crustal contamination and sulfide segregation. Chem. Geol. 243, 317–343.
Wang, C.Y., Zhou, M.F., Zhao, D.G., 2008. Fe–Ti–Cr oxides from the Permian Xinjie mafic–ultramafic layered intrusion in the Emeishan Large Igneous Province, SW China: crystallization from Fe- and Ti-rich basaltic magmas. Lithos 102, 198–217.
Watson, E.B., 1976. Two-liquid partition coefficients: experimental data and geochemical implications. Contrib. Miner. Petrol. 56, 119–134.
Xiao, L., Xu, Y.G., He, B., 2003. Emei mantle plume–subcontinental lithosphere interaction: Sr–Nd and O isotopic evidences from low-Ti and high-Ti basalts. Geol. J. China Univ. 9, 207–217 (in Chinese).
Xiao, L., Xu, Y.G., Mei, H.J., Zheng, Y.F., He, B., Pirajno, F., 2004a. Distinct mantle sources of low-Ti and high-Ti basalts from the western Emeishan Large Igneous Province, SW China: implications for plume–lithosphere interaction. Earth Planet. Sci. Lett. 228, 525–546.
Xiao, L., Xu, Y.G., Xu, J.F., He, B., Pirajno, F., 2004b. Chemostratigraphy of flood basalts in the Garze-Litang region and Zongza block: implications for western

extension of the Emeishan Large Igneous Province, SW China. Acta Geol. Sin. (English Edition) 78, 61–67.
Xu, Y.G., Chung, S.L., Jahn, B.M., Wu, G.Y., 2001. Petrologic and geochemical constraints on the petrogenesis of mian-Triassic Emeishan flood basalts in southwestern China. Lithos 58, 145–168.
Xu, Y.G., Luo, Z.Y., Huang, X.L., He, B., Xiao, L., Xie, L.W., Shi, Y.R., 2008. Zircon U–Pb and Hf isotope constraints on crustal melting associated with the Emeishan mantle plume. Geochim. Cosmochim. Acta 72, 3084–3104.
Yao, P.H., Wang, K.N., Du, C.L., Lin, Z.T., Song, X., 1993. Records of China's Iron Ore Deposits. Metallurgical Industry Press, Beijing, pp. 638–641 (in Chinese).
Zhang, Z.C., 2009. A discussion on some important problems concerning the Emeishan large igneous province. Geol. China 36, 634–646 (in Chinese with English abstract).
Zhang, Z.Q., Lu, J.R., Tang, S.H., 1999. Sm–Nd ages of the Panxi layered basic–ultrabasic intrusions in Sichuan. Acta Geol. Sci. 73, 263–271 (in Chinese).
Zhang, Z.C., Mahoney, J.J., Mao, J., Wang, F., 2006. Geochemistry of picritic and associated basalt flows of the western Emeishan flood basalt province, China. J. Petrol. 47, 1997–2019.
Zhang, Z.C., Hao, Y.L., Ai, Y., Li, Y., Zhao, L., 2009a. Phase equilibria constraints on relations of ore-bearing intrusions with flood basalts in the Panxi Region, SW China. Acta Geol. Sin. 83, 295–309.
Zhang, Z.C., Mao, J., Saunders, A.D., Li, Y., Zhao, L., 2009b. Petrogenetic modelling of three mafic–ultramafic layered intrusions in the Emeishan large igneous province, SW China, based on isotopic and bulk chemical constraints. Lithos 113, 369–392.
Zhang, X.Q., Song, X.Y., Chen, L.M., Xie, W., Yu, S.Y., Zheng, W.Q., Deng, Y.F., Zhang, J.F., Gui, S.G., 2012. Fractional crystallization and the formation of thick Fe–Ti–V oxide layers in the Baima layered intrusion, SW China. Ore Geol. Rev. 49, 96–108.
Zhong, H., Zhu, W.G., 2006. Geochronology of layered mafic intrusions from the Pan–Xi area in the Emeishan large igneous province, SW China. Miner. Deposita 41, 599–606.
Zhong, H., Zhou, X.H., Zhou, M.F., Sun, M., Liu, B.G., 2002. Platinum-group element geochemistry of the Hongge Fe–V–Ti deposit in the Pan–Xi area, southwestern China. Miner. Deposita 37, 226–239.
Zhong, H., Yao, Y., Hu, S.F., Zhou, X.H., Liu, B.G., Sun, M., Zhou, M.F., Viljoen, M.J., 2003. Trace-element and Sr–Nd isotopic geochemistry of the PGE-bearing Hongge Layered intrusion, Southwestern China. Int. Geol. Rev. 45, 371–382.
Zhong, H., Yao, Y., Prevec, S.A., Wilson, A.H., Viljoen, M.J., Viljoen, R.P., Liu, B.G., Luo, Y.N., 2004. Trace-element and Sr–Nd isotopic geochemistry of the PGE-bearing Xinjie layered intrusion in SW China. Chem. Geol. 203, 237–252.
Zhong, H., Hu, R.Z., Wilson, A.H., Zhu, W.G., 2005. Review of the link between the Hongge layered intrusion and the Emeishan flood basalts, southwest China. Int. Geol. Rev. 47, 971–985.
Zhou, M.F., Malpas, J., Song, X.Y., Robinson, P.T., Sun, M., Kennedy, A.K., Lesher, C.M., Keays, R.R., 2002. A temporal link between the Emeishan large igneous province (SW China) and the end-Guadalupian mass extinction. Earth Planet. Sci. Lett. 196, 113–122.
Zhou, M.F., Robinson, P.T., Lesher, C.M., Keays, R.R., Zhang, C.J., Malpas, J., 2005. Geochemistry, petrogenesis and metallogenesis of the Panzhihua gabbroic layered intrusion and associated Fe–Ti–V oxide deposits, Sichuan Province, SW China. J. Petrol. 46, 2253–2280.
Zhou, M.F., Zhao, J.H., Qi, L., Su, W.C., Hu, R.Z., 2006. Zircon U–Pb geochronology and elemental and Sr–Nd isotope geochemistry of Permian mafic rocks in the Funing area, SW China. Contrib. Miner. Petrol. 151, 1–19.
Zhou, M.F., Arndt, N.T., Malpas, J., Wang, C.Y., Kennedy, A.K., 2008. Two magma series and associated ore deposit types in the Permian Emeishan Large Igneous Province, SW China. Lithos 103, 352–368.
Zhou, M.F., Chen, W.T., Wang, C.Y., Prevec, S.A., Liu, Patricia P., Howarth, G.H., 2013. Two stages of immiscible liquid separation in the formation of Panzhihua-type Fe–Ti–V oxide deposits, SW China. Geosci. Front. 4, 481–502.
Zindler, A., Hart, S., 1986. Chemical geodynamics. Annu. Rev. Earth Planet. Sci. 14, 493–571.